2019

HIV-1 and SIV Infection are associated with early loss of lung interstitial CD4+ T cells and dissemination of pulmonary tuberculosis

Shabaana A. Khader

et al

Report

Cell Reports

HIV-1 and SIV Infection Are Associated with Early Loss of Lung Interstitial CD4+ T Cells and Dissemination of Pulmonary Tuberculosis

Graphical Abstract

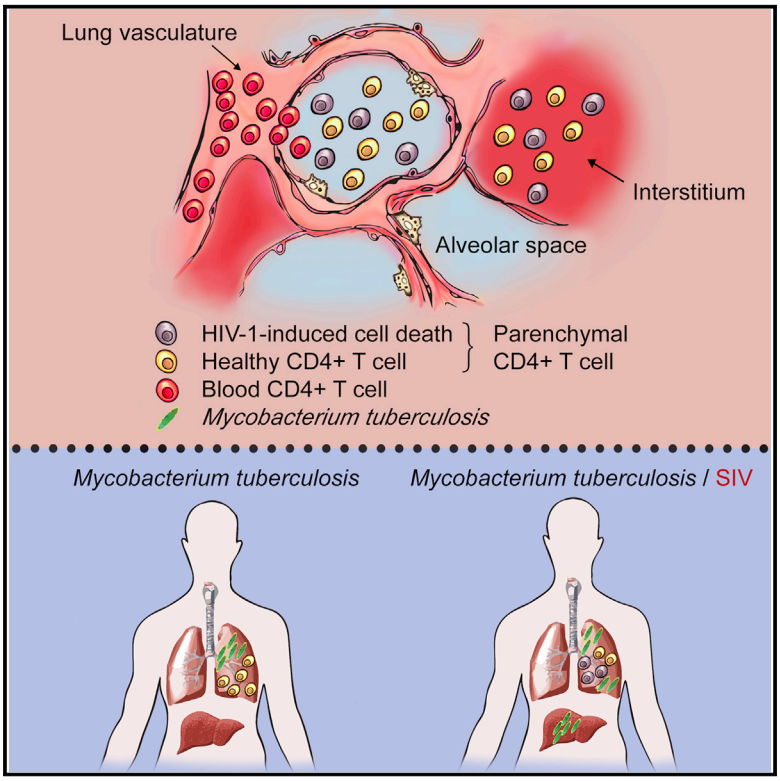

Authors

Björn Corleis, Allison N. Bucsan, Maud Deruaz, ..., Shabaana A. Khader, Deepak Kaushal, Douglas S. Kwon

Correspondence

bcorleis@mgh.harvard.edu

In Brief

Corleis et al. show that lung parenchymal CD4+ T cells are permissive to HIV-1-dependent cell death. CD4+ T cell loss is highly significant in the interstitium but not the alveolar space, and loss of interstitial CD4+ T cells is associated with extrapulmonary dissemination of *M. tuberculosis*.

Highlights

- Lung interstitial CD4+ T cells are highly permissive to HIV-1-induced cell death
- Alveolar CD4+ T cell numbers are not significantly altered with HIV-1 infection
- SIV infection leads to interstitial CD4+ T cell depletion during pulmonary TB
- Lung interstitial CD4+ T cell loss is associated with disseminated TB

Corleis et al., 2019, Cell Reports *26*, 1409–1418
February 5, 2019
https://doi.org/10.1016/j.celrep.2019.01.021

CellPress

Cell Reports
Report

HIV-1 and SIV Infection Are Associated with Early Loss of Lung Interstitial CD4+ T Cells and Dissemination of Pulmonary Tuberculosis

Björn Corleis,[1,9,*] Allison N. Bucsan,[2,3] Maud Deruaz,[1,4] Vladimir D. Vrbanac,[1,4] Antonella C. Lisanti-Park,[1] Samantha J. Gates,[1] Alice H. Linder,[1] Jeffrey M. Paer,[1] Gregory S. Olson,[1] Brittany A. Bowman,[1] Abigail E. Schiff,[1] Benjamin D. Medoff,[4,5] Andrew M. Tager,[1,4,5] Andrew D. Luster,[4] Shabaana A. Khader,[6] Deepak Kaushal,[2,7] and Douglas S. Kwon[1,8]

[1]Ragon Institute of MGH, MIT, and Harvard, Massachusetts General Hospital, Harvard Medical School, Boston, MA, USA
[2]Tulane National Primate Research Center, Covington, LA, USA
[3]Department of Microbiology and Immunology, Tulane University School of Medicine, New Orleans, LA, USA
[4]Center for Immunology and Inflammatory Diseases, Massachusetts General Hospital and Harvard Medical School, Charlestown, MA, USA
[5]Division of Pulmonary and Critical Care Medicine, Massachusetts General Hospital, Boston, MA, USA
[6]Department of Molecular Microbiology, Washington University School of Medicine, St. Louis, MO, USA
[7]Southwest National Primate Research Center, San Antonio, TX, USA
[8]Division of Infectious Diseases, Massachusetts General Hospital, Boston, MA, USA
[9]Lead Contact
*Correspondence: bcorleis@mgh.harvard.edu
https://doi.org/10.1016/j.celrep.2019.01.021

SUMMARY

Lung interstitial CD4+ T cells are critical for protection against pulmonary infections, but the fate of this population during HIV-1 infection is not well described. We studied CD4+ T cells in the setting of HIV-1 infection in human lung tissue, humanized mice, and a *Mycobacterium tuberculosis* (*Mtb*)/simian immunodeficiency virus (SIV) nonhuman primate co-infection model. Infection with a CCR5-tropic strain of HIV-1 or SIV results in severe and rapid loss of lung interstitial CD4+ T cells but not blood or lung alveolar CD4+ T cells. This is accompanied by high HIV-1 production in these cells *in vitro* and *in vivo*. Importantly, during early SIV infection, loss of lung interstitial CD4+ T cells is associated with increased dissemination of pulmonary *Mtb* infection. We show that lung interstitial CD4+ T cells serve as an efficient target for HIV-1 and SIV infection that leads to their early depletion and an increased risk of disseminated tuberculosis.

INTRODUCTION

HIV-1 infection results in loss of circulating CD4+ T cells, but only after years of untreated infection (Okoye and Picker, 2013). Investigation of HIV-1 and simian immunodeficiency virus (SIV) revealed severe CD4+ T cell depletion in the gut early after infection before significant loss of cells in the circulation or secondary lymph nodes (Brenchley et al., 2004; Li et al., 2005). Several studies have examined the effect of HIV-1 on lung CD4+ T cells obtained from bronchoalveolar lavage (BAL) as a method to sample the alveolar space as a proxy for the lung parenchyma. These studies reported minimal to no CD4+ T cell loss during acute or chronic HIV-1 infection in the alveolar space. This may in part be due to concomitant HIV-1-induced lymphocyte alveolitis, which could partially compensate for CD4+ T cell loss (Brenchley et al., 2008; Bunjun et al., 2017; Knox et al., 2010; Neff et al., 2015). Few studies have examined human lung interstitial CD4+ T cells, which are distinct from those in the alveolar space and are believed to be critical for providing protection against respiratory infections such as influenza and tuberculosis (TB) (Sakai et al., 2014; Zens et al., 2016). Because of the difficulty of assessing lung interstitial CD4+ T cells, our understanding of the effect of HIV-1 infection on this population of protective tissue-resident cells remains incomplete.

Mucosal CD4+ T cells constitute a large reservoir of HIV-1 target cells because of their high baseline activation state and expression of the HIV-1 entry co-receptor CCR5. HIV-1 strains that use CCR5 (CCR5-tropic) are primarily responsible for the establishment of infection and generally predominate until development of late-stage disease (Okoye and Picker, 2013). In contrast, the appearance of HIV-1 strains that use the co-receptor CXCR4 (CXCR4-tropic) is associated with progression to AIDS and depletion of CXCR4-expressing memory CD4+ T cells in secondary lymphoid organs (SLOs) (Doitsh et al., 2014; Penn et al., 1999). Lung CD4+ T cells express both CCR5 and CXCR4 (Purwar et al., 2011), but the susceptibility of these cells to HIV-1 and subsequent cell death have not been well characterized. This is particularly important because increased susceptibility to some respiratory infections, such as *Mycobacterium tuberculosis* (*Mtb*), has been reported early in HIV-1 disease, before systemic immune impairment is evident (Diedrich and Flynn, 2011).

Animal models of human pulmonary *Mtb* infection have identified a key role for CD4+ T cells in protecting against active TB (ATB) (Mogues et al., 2001). HIV-1 co-infection increases the risk for ATB by 20- to 40-fold (Lawn and Zumla, 2011), with high rates of extrapulmonary disseminated TB associated with unfavorable treatment outcomes and high mortality rates

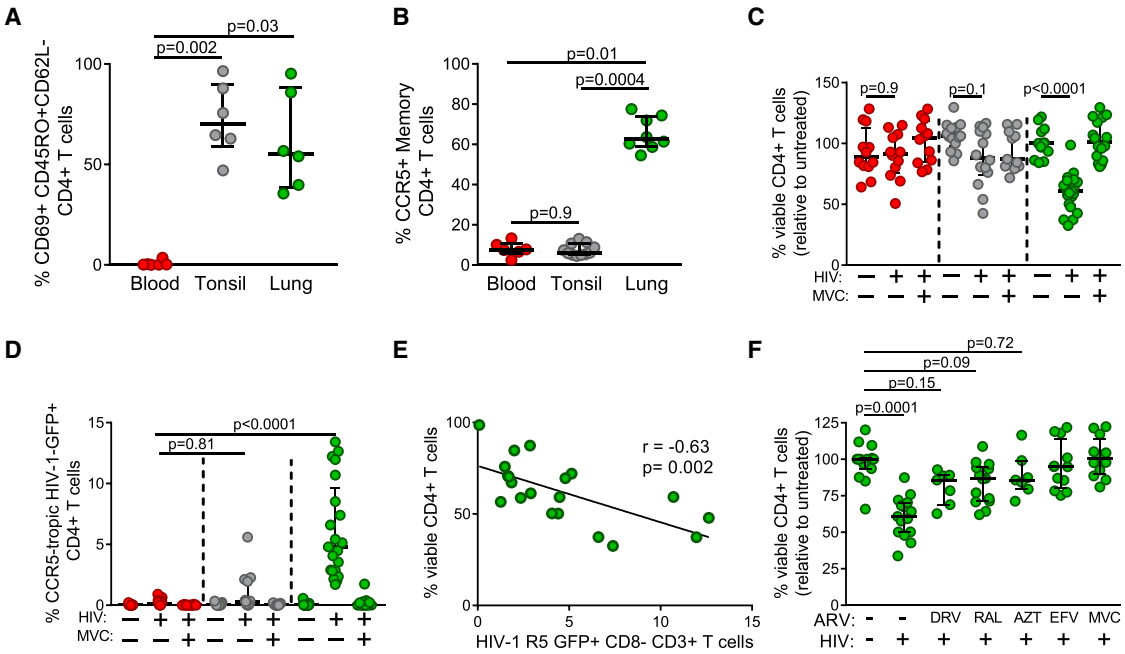

Figure 1. CCR5-Tropic HIV-1 Infection Induced Severe Depletion of Human Lung CD4+ T Cells

Single-cell suspensions were obtained from human lung, tonsil, and blood samples.

(A and B) The frequency of (A) T_{RM}-like CD4+ cells (TCRα/β+CD45RO+CD62L−CD25−CD69+) and (B) HIV-1 co-receptor CCR5+ memory CD4+ T cells was determined by flow cytometry.

(C–F) 0.5 × 10^6 cells were cultured in a V-bottom 96-well plate, and, where indicated, cells were incubated with antiretroviral (ARV) drugs (DRV, darunavir [a protease inhibitor]; RAL, raltegravir [an integrase inhibitor]; AZT, zidovudine [a reverse transcriptase (RT) inhibitor]; EFV, efavirenz [an RT inhibitor]; MVC, maraviroc [a CCR5 antagonist]) before infection with CCR5-tropic NL4-3 GFP HIV-1 and analyzed by flow cytometry.

(C) The percentage of viable CD4+ T cells was determined relative to untreated cells.

(D) The percentage of productively infected CD4+ T cells was determined by analyzing HIV-1 GFP+ CD4+ T cells.

(E) Correlation between percentage of viable CD4+ T cell and productively infected cells.

(F) Percentage of viable CD4+ T cells in mock-infected, HIV-1-infected, and HIV-1-infected samples pre-incubated with different ARVs.

The p values were measured by (A–D and F) Kruskal-Wallis and Dunn's multiple comparisons tests or (E) by Spearman r test. Scatterplots are labeled with median and interquartile range. Each data point represents the average of duplicates from one subject.

See also Figure S1.

(Kerkhoff et al., 2017). The risk for ATB generally correlates with the decrease in circulating CD4+ T cells (Lawn and Zumla, 2011; Sonnenberg et al., 2005). However, early in HIV-1 infection, individuals are at increased risk of ATB before significant loss of peripheral CD4+ T cells, suggesting that loss of CD4+ T cells in the circulation may not entirely reflect their depletion at the site of *Mtb* infection in the lung (Kerkhoff et al., 2017; Sonnenberg et al., 2005). Tissue-resident memory-like (T_{RM}-like) CD4+ T cells in the lung interstitium have a higher protective capacity against TB than *Mtb*-specific T cells in the circulation (Sallin et al., 2017). Whether HIV-1 infection results in depletion of protective CD4+ T cells in the lung interstitium and whether this is associated with HIV-1-induced susceptibility to active or disseminated TB is not well characterized.

We show that HIV-1 infection induces severe and early CD4+ T cell depletion in the lung interstitium using *ex vivo* infection of human CD4+ T cells from lung tissue and *in vivo* HIV-1 infection in a humanized mouse model. In contrast, alveolar CD4+ T cell numbers are only marginally affected by HIV-1 infection. We further demonstrate that early loss of lung interstitial, but not alveolar, CD4+ T cells during SIV infection of nonhuman primates (NHPs) is associated with dissemination of *Mtb* to extrapulmonary organs during latent TB infection (LTBI). These findings indicate that lung interstitial CD4+ T cell loss during early lentiviral infection is significantly underestimated by sampling of the alveolar space and that loss of these cells may contribute to the increased risk of *Mtb* dissemination seen in those with early HIV-1 infection.

RESULTS

CCR5-Tropic HIV-1 Induced Severe Depletion of Human Lung CD4+ T Cells

We examined lymphocytes collected from human lungs, tonsils, and blood for CD4+ T cell phenotypes and HIV-1 co-receptor expression. Consistent with other reports, CD4+ T cells in human lungs and tonsils were enriched for CD69+CD45RO+CD62L− T_{RM}-like cells (Figure 1A; Kumar et al., 2017; Mahnke et al., 2013). However, only lung memory CD4+ T cells demonstrated high expression levels of the HIV-1 co-receptor CCR5

(Figure 1B). Given the high frequency of CCR5+ T_{RM}-like cells in the lung, we surmised that these cells would be highly susceptible to CCR5-tropic HIV-1 infection. We infected lung-, blood-, and tonsil-derived lymphocytes with CCR5-tropic HIV-1 encoding a GFP reporter and analyzed the frequency of infected cells. For human lung tissue, we observed a significant decrease in viable CD4+ T cells (Figure 1C; Figure S1A) but not CD8+ T cells (Figure S1B), accompanied by a higher frequency of HIV-1 CCR5-tropic-infected CD4+ T cells compared with tonsils and peripheral blood mononuclear cells (PBMCs) (Figure 1D). Viral replication and the loss of viable CD4+ T cells were dependent on HIV-1 co-receptor-mediated entry because the CCR5 receptor antagonist maraviroc inhibited CD4+ T cell loss and viral replication (Figures 1C and 1D). In contrast, tonsil CD4+ T cells were more susceptible to productive infection and depletion by a CXCR4-tropic virus (Figures S1C and S1D). Following *in vitro* infection, the decrease in viable CD4+ T cells correlated with the frequency of productively infected HIV-1 CCR5-tropic GFP+ CD4+ T cells (Figure 1E). Next we investigated viral functions required to induce significant cell loss by testing antiretrovirals (ARVs) that target different stages of the HIV-1 life cycle. The protease inhibitor darunavir (DRV), the integrase inhibitor raltegravir (RAL), the nucleoside analog reverse transcriptase (RT) inhibitor zidovudine (AZT), the non-nucleoside analog RT inhibitor efavirenz (EFV), and the viral entry inhibitor maraviroc (MVC) were all able to reduce HIV-1-induced CD4+ T cell loss with no significant difference in viable CD4+ T cells compared with mock-infected controls (Figures 1F and S1E). Productive HIV-1 infection has been reported to induce caspase-3-dependent cell death, whereas abortive infection induces caspase-1 or inflammasome-mediated pyroptosis (Doitsh et al., 2014; Jekle et al., 2003). The pan caspase inhibitor Z-VAD and the caspase-3 inhibitor Z-DEVD fully rescued HIV-1-induced CD4+ T cell loss, whereas the caspase-1 inhibitor had no effect (Figure S1F). Likewise, CCR5-tropic HIV-1 induced secretion of the pro-inflammatory cytokine CXCL10 but not the caspase-1 or inflammasome-induced cytokine interleukin-1β (IL-1β) (Figures S1G and S1I). Together, our data indicate that lung CD4+ T cells are highly permissive to productive viral infection with CCR5-tropic HIV-1, which caused rapid caspase-3-mediated CD4+ T cell death in human lung tissue.

Lung Interstitial CD4+ T Are Cells Severely Depleted during Acute HIV-1 Infection *In Vivo*

Our *ex vivo* experiments with human lung tissue indicated that lung CD4+ T cells are more affected by HIV-1 than previously estimated from studies of human BAL (Bunjun et al., 2017). The humanized mouse has been used to study early HIV-1 infection in tissue and, therefore, offered an opportunity to investigate depletion of BAL and lung interstitial CD4+ T cells following HIV-1 infection *in vivo* (Deruaz et al., 2017). Humanized mice were challenged intravaginally with CCR5-tropic HIV-1 JR-CSF or saline control. Lung CD4+ T cells were characterized 4 and 7 weeks after infection, at stages that reflect acute and early chronic HIV-1 infection, respectively (Dudek and Allen, 2013; Dudek et al., 2012; McMichael et al., 2010). CD4+ T cells were only significantly depleted in the lung interstitium, where they were reduced by 6.6-fold at week 7 (Figures 2A–2D). This depletion was significantly higher compared with paired BAL samples at week 4 and week 7 (Figures 2E and 2F). In BAL samples, we observed a trend for increased BAL CD8+ T cell numbers, with a significantly higher fold increase of BAL CD8+ T cells from HIV+ humanized mice at weeks 4 and 7 compared with paired lung interstitial CD8+ T cells (Figures S2A–S2F). Further, the number of T cells (CD4+ and CD8+ T cells combined) correlated with the presence of the T cell-recruiting chemokine CXCL10 in BAL but not the lung interstitium, suggesting recruitment of T cells to the alveolar space (Figures S2G and S2H). Using quantitative immunohistochemistry, we confirmed severe depletion of lung interstitial CD4+ T cells *in vivo* (Figures 2G–2I). Given that CD4+ T cell loss in lung tissue *in vitro* was accompanied by a high frequency of productively infected CD4+ T cells, we measured the HIV-1 viral load in the lungs and spleens of HIV-1-infected humanized mice. We observed that the viral load in total lung tissue was significantly higher compared with the spleen 7 weeks after infection (Figure 3A). Further, we also quantified viral RNA from sorted CD4+ T cells and CD14+ monocytes from spleen and lung tissue and found 5.5-fold more HIV-1 gag RNA in lung versus spleen CD4+ T cells, whereas detection of viral RNA from sorted monocytes was below the limit of detection in most samples (Figure 3B). Additionally, we stained HIV-1 p24 protein in tissue sections and found a significantly higher ratio of p24+:CD4+ cells in lung tissue sections compared with the spleen (Figures 3C and 3D). Thus, HIV-1 infection in humanized mice with a CCR5-tropic HIV-1 strain resulted in high levels of productive infection and profound loss of CD4+ T cells in the lung interstitium, where depletion was more severe than in the blood, spleen, and alveolar space.

CD45iv− Lung Interstitial CD4+ T Cells Are Most Significantly Depleted by HIV-1

CD4+ interstitial T_{RM}-like cells are characterized by their effector memory phenotype, expression of CD69, high expression of CD11a, and their inaccessibility to antibodies in the circulation introduced by intravenous injection (CD45iv−) (Anderson et al., 2014). To further differentiate resident interstitial versus vascular CD4+ T cells in the lungs of the humanized mouse, we *in vivo*-labeled vascular cells with an antibody binding to human CD45 3 min before sacrificing the mice and analyzed CD45iv− CD4+ interstitial T_{RM}-like cells by flow cytometry (Figure S3). Lung T cells consisted of a CD45iv− and CD45iv+ population, whereas other compartments were primarily CD45iv− (BAL and spleen) or CD45iv+ (blood) (Figure 4A). CD45iv− CD4+ T cells in the lungs showed significantly higher loss compared with blood CD4+ T cell loss (Figure 4B). CD45iv− and CD45iv+ lung CD4+ T cells had an increased frequency of memory T cells and the lung recruiting chemokine receptor CXCR3 (Figures S4A and S4B). However, only lung interstitial CD45iv− CD4+ T cells had high expression of the T_{RM} cell markers CD69 (Figure 4C) and CD11a (Figure S4C) and showed higher expression of the HIV-1 co-receptor CCR5 compared with vascular CD45iv+ lung CD4+ T cells (Figure 4D). Furthermore, lung CD45iv− CD4+ T cells had the highest frequency of HIV-1 p24+ cells, and the number of lung interstitial CD45iv− CD4+ T cells, but not blood CD4+ T cells, correlated with the frequency

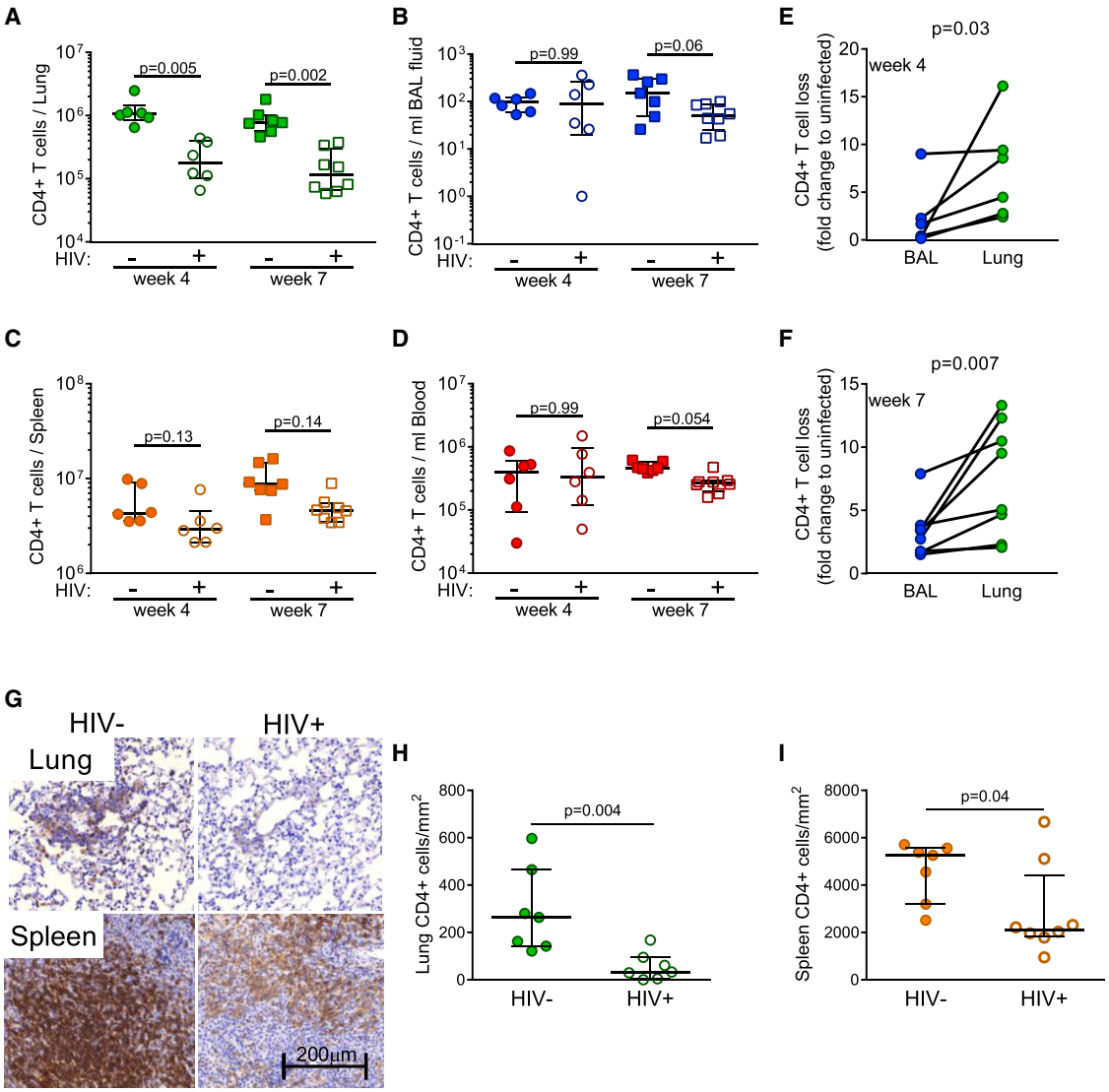

Figure 2. HIV-1 Infection Results in Severe Depletion of Lung Interstitial CD4+ T Cells *In Vivo*

Humanized mice from 2 different batches were intravaginally infected with 50,000 infectious particles of HIV-1 (JR-CSF) (n = 14) or left uninfected as controls (n = 13).

(A–D) 4 and 7 weeks after infection, cells from (A) the lung interstitium, (B) BAL, (C) the spleen, and (D) the blood were analyzed for CD4+ T cell loss by comparing CD4+ T cell numbers with uninfected control animals using flow cytometry.

(E and F) CD4+ T cell loss in paired BAL and lung samples was analyzed as fold change compared with the median CD4+ T cell count of uninfected animals (E) 4 weeks or (F) 7 weeks after infection.

(G) Depletion of CD4+ T cells 7 weeks after infection in lungs compared with the spleen was confirmed by immunohistochemistry (IHC) staining for CD4.

(H and I) CD4+ cells in (H) the lungs and (I) the spleen were quantified using Histoquest software.

The p values were measured by Kruskal-Wallis and Dunn's multiple comparisons tests and (H and I) Mann-Whitney U test. Scatterplots are labeled with median and interquartile range. Each data point represents one humanized mouse sample.

See also Figure S2.

of HIV-1 p24+ CD4+ T cells (Figure S4D; Figures 4E and 4F). Taken together, CD45 *in vivo* labeling revealed the presence of a CD4+ CD45iv−CD45RO+CD62L−CD69+CD11a^{high} interstitial T_{RM}-like cell population in the lung, which demonstrated severe depletion with HIV-1 infection that was not reflected by sampling of cells in the alveolar space.

Mtb/SIV Co-infection in NHPs Leads to Severe CD4+ T Cell Depletion in the Lungs and Increased Disseminated TB

Increased risk of ATB correlates with the loss of circulating CD4+ T cells during AIDS progression. However, HIV infection increases the risk for ATB before significant CD4+ T cell loss in

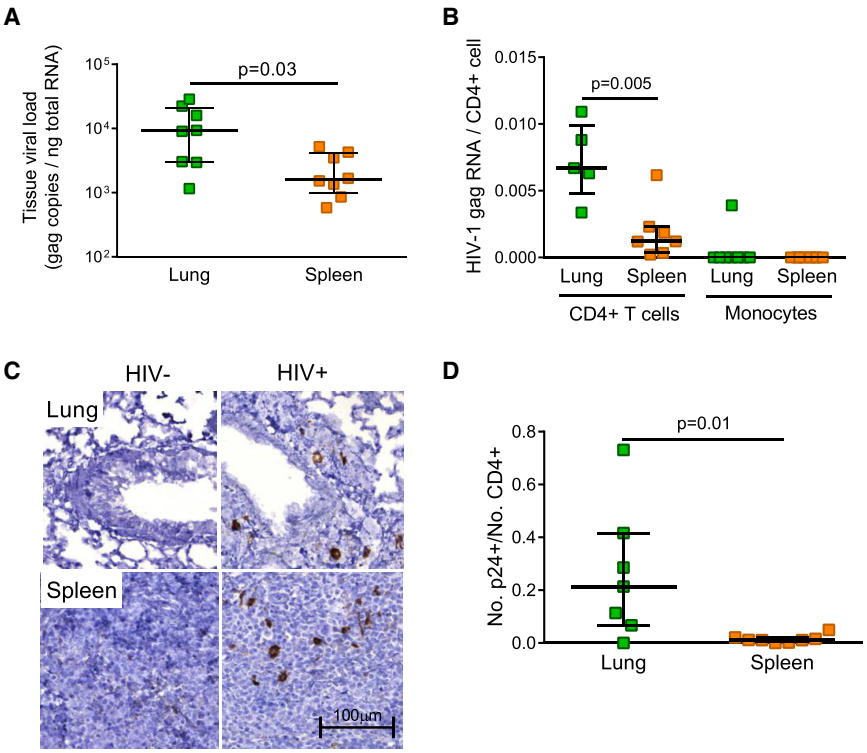

Figure 3. CD4+ T Cells in the Lungs Are Highly Susceptible to Productive HIV-1 Infection *In Vivo*

(A and B) 7 weeks after infection, RNA was extracted from lung and spleen (A) total tissue or (B) from sorted CD4+ T cells from the lungs and spleen. HIV-1 RNA was detected by HIV-1 gag qPCR and quantified by using a linear HIV-1 standard and normalized to CD4+T cell counts.

(C and D) Production of virus in lung CD4+ cells was confirmed by protein staining of HIV-1 p24 using IHC (C). The ratio of p24+ cells:CD4+ cells in the lungs and spleen was quantified using Histoquest software (D).

The p values were measured by (A and D) Mann-Whitney U test and (B) Kruskal-Wallis and Dunn's multiple comparisons tests. Scatterplots are labeled with median and interquartile range. Each data point represents one humanized mouse sample.

the blood (Sonnenberg et al., 2005). We hypothesized that, during early HIV-1 infection, lung interstitial CD4+ T cell loss is associated with TB disease progression. The humanized mouse is highly susceptible to even non-pathogenic mycobacterium infection, and the generalizability of HIV-1-induced lung interstitial CD4+ T cell depletion is unclear (Lee et al., 2013). We therefore used the NHP *Mtb*/SIV co-infection model. NHPs were infected with a low dose of *Mtb* CDC1551 to establish LTBI 9 weeks before co-infecting a subgroup with SIVmac239 for 11–13 weeks. SIV infection significantly increased reactivation of LTBI (Figure S5A). At the time of necropsy, the number of bulk and effector memory lung interstitial CD4+ T cells was significantly reduced (Figure 5A; Figure S5B), whereas CD4+ T cells in BAL, blood, bronchial lymph nodes (Br LNs), and the spleen were not significantly decreased (Figures 5B and 5C; Figures S5C–S5F), consistent with our findings with human lung tissue and humanized mice. Lung interstitial CD4+ T cell loss was significantly higher compared with paired BAL samples (Figure 5D), and BAL CD8+ T cell numbers showed a trend of increased numbers in SIV-co-infected compared with SIV-uninfected animals (Figure S5G).

Patients with clinical HIV-1/TB co-infection often present with extrapulmonary TB (Lawn and Gupta-Wright, 2016). Because CD4+ T_{RM}-like cells have been described as important for control of pulmonary *Mtb* infection, we hypothesized that the early loss of lung interstitial CD4+ T cells in NHPs latently infected with *Mtb* would also contribute to the dissemination of *Mtb* to other organs. We found an increased extrapulmonary *Mtb* burden in SIV-infected animals compared with those that were uninfected, with a significantly higher bacterial burden in the liver (Figure 5E) and with similar trends for the spleen and kidneys (Figures S5H and S5I). Interestingly, decreasing lung interstitial CD4+ T cell numbers significantly correlated with *Mtb* burden in the liver (Figure 5F) and spleen (Figure S5J) in NHPs with LTBI. In comparison, BAL or blood CD4+ T cells did not correlate with extrapulmonary burden (Figures S5K and S5L). In summary, early SIV infection resulted in severe depletion of lung interstitial CD4+ T cells but not those in the alveoli. Importantly, this lung interstitial CD4+ T cell loss was strongly associated with dissemination of pulmonary TB before reactivation of LTBI.

DISCUSSION

HIV-1 primarily infects CD4+ T cells, which leads to the loss of this important arm of the immune response and contributes to increased susceptibility to opportunistic infections. Our study revealed that, unlike CD4+ T cells in the alveolar space or circulation, lung interstitial CD4+ T cells are severely depleted by HIV-1 early in infection in human lung tissue *ex vivo,* in humanized mice *in vivo*, and by SIV in NHPs. HIV-1-induced lung interstitial CD4+ T cell depletion was accompanied by high virus production and was rescued by ARVs or caspase-3 inhibition *in vitro*. Further, CD45 *in vivo* labeling revealed that lung interstitial CD4+ T_{RM}-like cells showed the highest HIV-1 infection rates, which was associated with their depletion. The severe loss of lung interstitial CD4+ T cells in *Mtb*/SIV co-infected NHPs correlated strongly with dissemination of *Mtb* into extrapulmonary organs.

Although mucosal CD4+ T cells in the intestinal tract have been reported to be depleted early during infection with HIV-1 or SIV, the fate of lung interstitial CD4+ T cells has been less well characterized. Here we describe early severe depletion of lung interstitial CD4+ T cells *in vitro* and in *vivo*, induced by HIV-1 in human cells and by SIV in NHPs. Previously, human studies of lung CD4+ T cells in HIV-infected subjects have

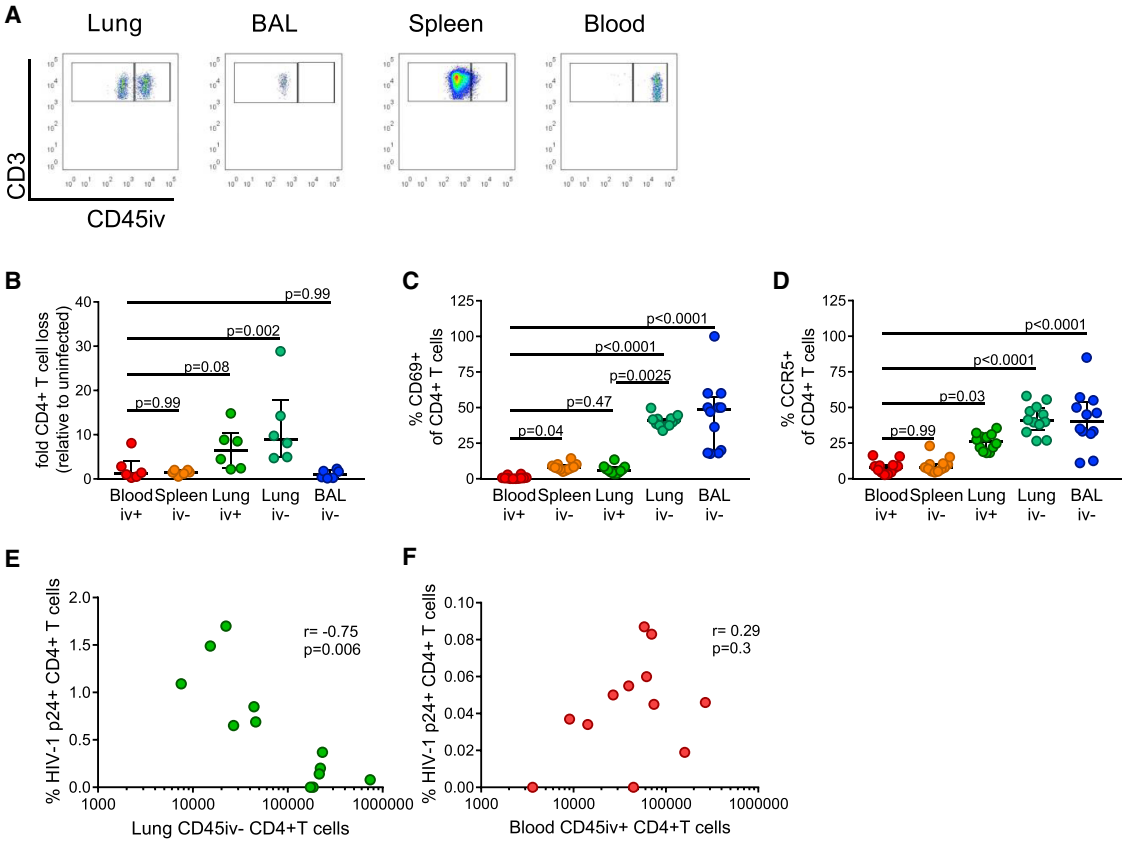

Figure 4. CD69+ Memory CD45iv− Lung Interstitial CD4+ T Cells Are Most Significantly Affected by HIV-1-Induced CD4+ T Cell Loss

HIV-1-infected humanized mice (n = 6) or uninfected control mice (n = 12) were labeled by injection of an anti-human CD45 antibody for 3 min prior to sacrifice. CD45iv– and positive CD4+ T cells were analyzed in the lungs, BAL, spleen, and blood by flow cytometry.

(A) Representative plots of CD45iv+ and CD45iv− CD4+ T cells in the lungs, BAL, spleen, and blood.

(B–D) The T_{RM}-like phenotype of CD45iv+ or CD45iv− CD4+ T cells was further characterized by flow cytometry.

(B) Fold lung CD4+T cell loss was analyzed by comparing CD4+ T cell numbers from infected with median uninfected control animals.

(C) The percentage of all CD4+ T cells with surface expression of CD69+ was analyzed by gating on viable CD4+ TCRα/β+CD45RO+CD62L−CD25− T cells.

(D) The percentage of all CD4+ T cells with surface expression of CCR5+ was analyzed by gating on viable CD4+ T cells.

(E and F) Correlation between intracellular HIV-1 p24+ CD4+ T cells 4 weeks after infection and number of (E) lung CD45iv− CD4+ T cell and (F) blood CD45iv+ CD4+ T cells.

The p values were measured by (A–D) Kruskal-Wallis and Dunn's multiple comparisons tests and (E and F) Spearman test. Scatterplots are labeled with median and interquartile range. Each data point represents one humanized mouse sample.

See also Figures S3 and S4.

used BAL as a surrogate for interstitial tissue cells and have suggested minimal or no depletion of CD4+ T cells in this compartment (Brenchley et al., 2008; Bunjun et al., 2017; Mwale et al., 2018). A study in NHPs reported transient BAL CD4+ T cell depletion that was rapidly reversed by infiltrating CD4+ T cells with increased anti-viral resistance (Verhoeven et al., 2014). Our studies in the humanized mouse and NHPs allowed us to simultaneously compare paired BAL and lung interstitial CD4+ T cells *in vivo*. Although BAL CD4+ T cells had a similar phenotype as lung interstitial T cells, the CD4+ T cell loss in BAL compared with SIV-uninfected NHPs was more comparable with the blood and spleen and consistent with the observations in BAL from human cohort studies. It is possible that the lymphocytic infiltration into alveoli during HIV-1 infection that has been described in humans and NHPs might compensate for CD4+ T cell loss. The observed differences in CD4+ T cell depletion in the lung interstitium versus BAL highlights that sampling of the alveolar space does not fully reflect HIV-1 infection of lung interstitial CD4+ T cells. Therefore, our data suggest that the severity of lung CD4+ T cell depletion has been underestimated, with early and severe lung CD4+ T cells depletion similar to those found in the gut.

Intestinal CCR5+ CD4+ effector memory T cells (T_{EM} cells) are a preferred target cell for HIV-1 replication *in vivo* (Dillon et al., 2016; Mattapallil et al., 2005; Steele et al., 2014; Veazey et al., 2000). We also found that enrichment of this cell type in the lungs had consequences for their susceptibility to HIV-1 infection and depletion. We showed that CCR5-tropic HIV-1 replication was high in these cells in the lung *in vitro*, whereas CXCR4-tropic HIV-1 efficiently replicated in tonsil CD4+ T cells. In both cases,

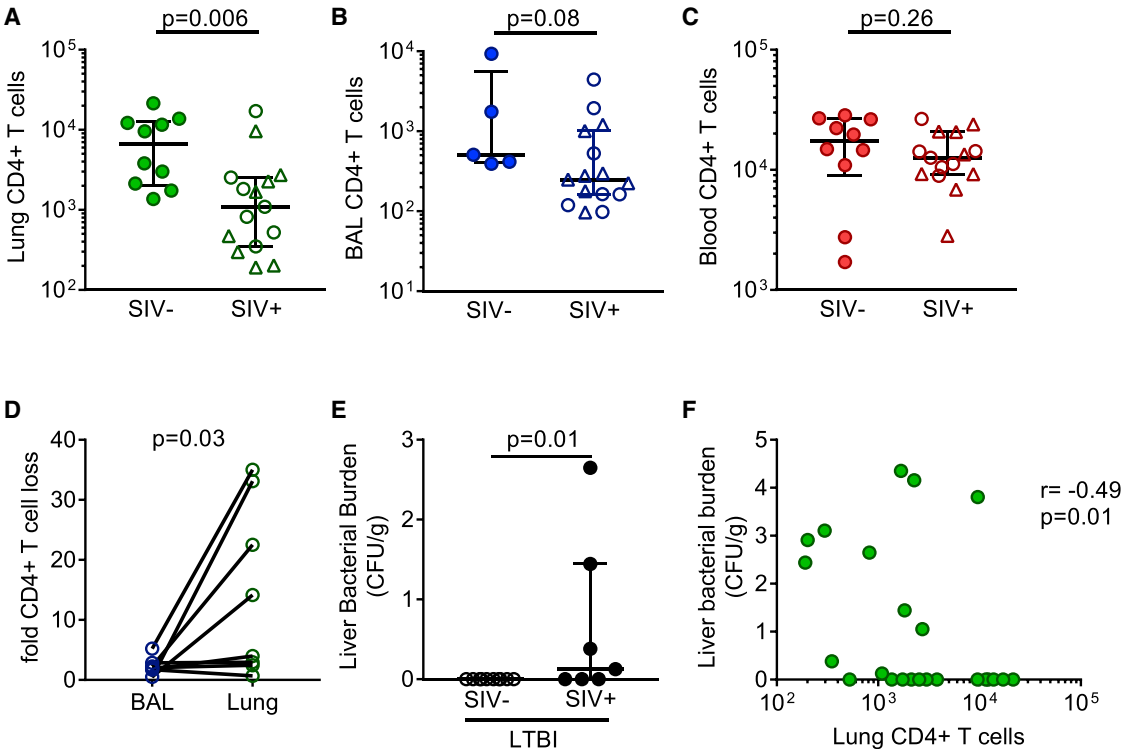

Figure 5. *Mtb*/SIV Co-infection in NHPs Leads to Severe CD4+ T Cell Depletion in the Lung Interstitium, which Is Associated with Increased Disseminated TB

Rhesus macaques were infected with *Mtb* CDC1551 via low-dose aerosol challenge to establish LTBI (n = 26). 9 weeks after *Mtb* infection, a subset of the NHPs (n = 15) was co-infected with SIVmac239. Necropsy was performed 20–22 weeks after *Mtb* infection or after TB reactivation with collection of the lungs, spleen, kidneys, and liver. BAL was performed prior to necropsy.

(A–C) None of the SIV-uninfected animals progressed from LTBI (circles) to active tuberculosis (ATB; triangles), whereas 8 animals in the SIV-infected group developed ATB. CD4+ T cell numbers in lung tissue (A), BAL (B), and blood (C) were assessed by flow cytometry.

(D) CD4+ T cell loss relative to the median in the CD4+ T cell count in SIV-uninfected NHPs in paired BAL and lung samples was determined.

(E) *Mtb* burden in the liver was measured in SIV-infected and uninfected NHPs, and lung interstitial CD4+ T cell numbers were correlated with liver CFUs/g tissue. The p values were measured by (A–C and E) Mann-Whitney U test, (D) Wilcoxon test, or (F) Spearman r test. Scatterplots are labeled with median and interquartile range. Each data point represents one NHP.

See also Figure S5.

the high frequency of productively infected CD4+ T cells was accompanied by severe CD4+ T cell loss. In contrast to mucosal tissue, CXCR4-tropic HIV-1 preferentially infected CD4+ T cells from SLOs, suggesting that viral replication at this site may be more relevant during later stages of infection in patients where the CXCR4-tropic virus has emerged (Doitsh et al., 2010; Glushakova et al., 1999; Grivel et al., 2007; Grivel et al., 2000a, 2000b). Inhibition of viral replication by ARVs or by a caspase-3 inhibitor was sufficient to completely rescue CD4+ T cell loss. Prior reports support our finding that productive infection of CD4+ T cells activates caspase-3-mediated cell death, whereas inflammasome and caspase-1 activity cause CD4+ T cell death during abortive infection (Badley et al., 2000; Doitsh et al., 2010; Li et al., 2005). The caspase-1 pyroptosis pathway in abortively infected cells was shown to be activated by the accumulation of viral cDNA, and treatment with the integrase inhibitor raltegravir did not rescue CD4+ T cell death (Monroe et al., 2014). However, these studies were conducted with the CXCR4-tropic virus and SLO-derived CD4+ T cells, which suggests that there are important differences in the mechanism of cell death in mucosal tissue versus SLOs. In contrast to SLOs, but similar to lung tissue, CD4+ T cells in the intestinal tract are highly susceptible to CCR5-tropic HIV-1 infection and HIV-1-mediated cell death early during infection (Brenchley et al., 2004; Li et al., 2005).

SIV infection in NHPs showed similar patterns for lung CD4+ T cell depletion as we observed for HIV-1 infection in lung tissue. We extended our findings by using the experimental NHP model for human LTBI to investigate the relevance of CD4+ T cell depletion for dissemination of *Mtb* infection. The NHP model reflects the high prevalence of *Mtb*/HIV-1 co-infection in sub-Saharan African countries, with the limitation that, in *Mtb*/HIV-1 co-infected humans, re-infection is more likely than reactivation (Andrews et al., 2012; Mahomed et al., 2011). We found that SIV significantly induced reactivation of LTBI and that, at the time of necropsy, only lung interstitial CD4+ T cell were severely depleted. Our data suggest that, during early viral infection, CD4+ T cells in BAL, circulation, and SLOs are

not significantly depleted and associated with ATB. The protective role of circulating CD4+ T cells in humans has been supported by the fact that ATB correlates with the decline of blood CD4+ T cells during chronic HIV-1 (Lawn et al., 2009). However, other reports have found that CD4+ T cells in the blood are not directly associated with protection against ATB. Adoptive intravenous transfer of *Mtb*-specific CD4+ T cells into the circulation of mice infected with *Mtb* for 1 week does not reduce the bacterial burden (Gallegos et al., 2008), and protection against ATB in Bacillus Calmette Guérin (BCG)-vaccinated adolescents does not correlate with circulating *Mtb*-specific CD4+ T cell responses (Kagina et al., 2010). We also did not find that depletion of lung interstitial CD4+ T cells correlated with reactivation of LTBI. Therefore, although CD4+ T cells are important for a protective immune response, reduced CD4+ T cell numbers in the blood or the lung interstitium alone may not explain increased susceptibility to TB in *Mtb*/HIV-co-infected patients. Location, phenotype, and their interaction with other cell types are likely also important for their protective role (Foreman et al., 2016; Sallin et al., 2017). However, our study is limited to the role of CD4+ T cells in HIV-1-associated TB. HIV-1 impairs other cell types, such as innate lymphoid cells, mucosa-associated invariant T cells, dendritic cells, and macrophages, which might all contribute to increased susceptibility to TB (Diedrich and Flynn, 2011; Kløverpris et al., 2016; Wong et al., 2013). HIV-1 infection is associated with extrapulmonary TB. We report that lung CD4+ T cell depletion correlated with extrapulmonary *Mtb* burden in *Mtb*/SIV co-infection, suggesting that lung interstitial CD4+ T cells are important for supporting a localized immune response to prevent dissemination of *Mtb*. We show an association between the severe loss of lung interstitial CD4+ T cells and disseminated TB early in infection, before loss of circulating CD4+ T cells. It has been reported that lung *Mtb*-specific CD4+ T cells produce tumor necrosis factor alpha (TNF-α), which is important in the maintenance of granuloma structures and prevention of disseminated *Mtb* (Lin et al., 2010). Whether specific SIV-mediated depletion of lung interstitial TNF-α+ CD4+ T cells could be a potential mechanism for lung CD4+ T cell-associated extrapulmonary TB should be further characterized.

In summary, HIV-1 and SIV infection of CD4+ T cells leads to their severe depletion at mucosal sites. This has been well established in the gut but less well characterized in the lung interstitium. Our findings show a discordance between characterization of the lung interstitium and alveoli following lentiviral infection. This distinction is important in the context of *Mtb* co-infection because CD4+ T cell loss in the lung interstitium, but not the alveolar space, is associated with extrapulmonary tuberculosis and may help explain the high prevalence of disseminated TB even in early HIV-1 infection.

STAR★METHODS

Detailed methods are provided in the online version of this paper and include the following:

- KEY RESOURCES TABLE
- CONTACT FOR REAGENT AND RESOURCE SHARING
- EXPERIMENTAL MODEL AND SUBJECT DETAILS
  - Human subjects
  - Humanized mouse
  - Non-human primates
  - Cell lines
- METHOD DETAILS
  - Human blood and tissue samples
  - HIV-1 *in vitro* infection assay
  - Flow cytometry
  - HIV-1 *in vivo* humanized mouse infection
  - HIV-1 gag RNA reverse transcriptase quantitative PCR (RT-qPCR)
  - Immunohistochemistry
  - Mycobacterium tuberculosis / SIV infection in nonhuman primates
- QUANTIFICATION AND STATISTICAL ANALYSIS

SUPPLEMENTAL INFORMATION

Supplemental Information includes five figures and two tables and can be found with this article online at https://doi.org/10.1016/j.celrep.2019.01.021.

ACKNOWLEDGMENTS

D.S.K. and B.D.M. were supported by the NHLBI (U01HL121827) and D.S.K. by the Burroughs Wellcome Fund. A.D.L. was supported by AI040618 and AI112521. This work was also supported by the Human Immune System Mouse Core subcontract (A.M.T., principal investigator) from the NIH Harvard University Center for AIDS Research (CFAR) and NIH/NIAID P30 AI060354 (Dr. Bruce Walker, principal investigator). A.E.S. was supported by awards T32GM007753 and F30HL134566-02 from the National Institute of General Medical Sciences. D.K. and S.A.K. were supported by AI111914, AI123780, AI111943, AI089323, HL106790, and RR026006. We would like to thank the pathology lab at MGH for tissue collection, Dr. Thorsten Mempel and Dr. Thomas Murooka for kindly providing NL4-3 GFP HIV-1, and the CFAR humanized mouse core for their service.

AUTHOR CONTRIBUTIONS

Conceptualization, B.C., M.D., A.M.T., and D.S.K.; Methodology, M.D., V.D.V., A.M.T., A.D.L., D.K., and S.A.K.; Validation, M.D., A.N.B., and B.C.; Formal Analysis, B.C., A.E.S., D.S.K., A.N.B., and S.A.K.; Investigation, B.C., A.C.L.-P., S.J.G., J.M.P., M.D., G.S.O., B.A.B., V.D.V., A.E.S., and A.N.B.; Resources, J.M.P., A.M.T., A.D.L., D.S.K., B.D.M., D.K., and S.A.K.; Data Curation, J.M.P. and B.C.; Writing – Original Draft, B.C. and D.S.K.; Writing – Review & Editing, B.C., D.S.K, A.D.L., M.D., D.S.K., A.N.B., A.C.L.-P., B.D.M., and B.A.B.; Visualization, B.C. and D.S.K.; Supervision, B.C., D.S.K., B.D.M., A.M.T., A.D.L., D.K., and S.A.K.; Funding Acquisition, A.E.S., A.M.T., A.D.L., D.S.K., D.K., and S.A.K.

DECLARATION OF INTERESTS

The authors declare no competing interests.

Received: August 16, 2018
Revised: November 25, 2018
Accepted: January 4, 2019
Published: February 5, 2019

REFERENCES

Anderson, K.G., Mayer-Barber, K., Sung, H., Beura, L., James, B.R., Taylor, J.J., Qunaj, L., Griffith, T.S., Vezys, V., Barber, D.L., and Masopust, D. (2014). Intravascular staining for discrimination of vascular and tissue leukocytes. Nat. Protoc. *9*, 209–222.

Andrews, J.R., Noubary, F., Walensky, R.P., Cerda, R., Losina, E., and Horsburgh, C.R. (2012). Risk of progression to active tuberculosis following reinfection with Mycobacterium tuberculosis. Clin. Infect. Dis. *54*, 784–791.

Badley, A.D., Pilon, A.A., Landay, A., and Lynch, D.H. (2000). Mechanisms of HIV-associated lymphocyte apoptosis. Blood *96*, 2951–2964.

Boutwell, C.L., Rowley, C.F., and Essex, M. (2009). Reduced viral replication capacity of human immunodeficiency virus type 1 subtype C caused by cytotoxic-T-lymphocyte escape mutations in HLA-B57 epitopes of capsid protein. J. Virol. *83*, 2460–2468.

Boutwell, C.L., Carlson, J.M., Lin, T.H., Seese, A., Power, K.A., Peng, J., Tang, Y., Brumme, Z.L., Heckerman, D., Schneidewind, A., et al. (2013). Frequent and variable cytotoxic-T-lymphocyte escape-associated fitness costs in the human immunodeficiency virus type 1 subtype B Gag proteins. J. Virol *87*, 3952–3965.

Brenchley, J.M., Schacker, T.W., Ruff, L.E., Price, D.A., Taylor, J.H., Beilman, G.J., Nguyen, P.L., Khoruts, A., Larson, M., Haase, A.T., and Douek, D.C. (2004). CD4+ T cell depletion during all stages of HIV disease occurs predominantly in the gastrointestinal tract. J. Exp. Med. *200*, 749–759.

Brenchley, J.M., Knox, K.S., Asher, A.I., Price, D.A., Kohli, L.M., Gostick, E., Hill, B.J., Hage, C.A., Brahmi, Z., Khoruts, A., et al. (2008). High frequencies of polyfunctional HIV-specific T cells are associated with preservation of mucosal CD4 T cells in bronchoalveolar lavage. Mucosal Immunol. *1*, 49–58.

Bunjun, R., Riou, C., Soares, A.P., Thawer, N., Müller, T.L., Kiravu, A., Ginbot, Z., Oni, T., Goliath, R., Kalsdorf, B., et al. (2017). Effect of HIV on the frequency and number of Mycobacterium tuberculosis-specific CD4+ T cells in blood and airways during latent M. tuberculosis infection. J. Infect. Dis. *216*, 1550–1560.

Deruaz, M., Murooka, T.T., Ji, S., Gavin, M.A., Vrbanac, V.D., Lieberman, J., Tager, A.M., Mempel, T.R., and Luster, A.D. (2017). Chemoattractant-mediated leukocyte trafficking enables HIV dissemination from the genital mucosa. JCI Insight *2*, e88533.

Diedrich, C.R., and Flynn, J.L. (2011). HIV-1/mycobacterium tuberculosis coinfection immunology: how does HIV-1 exacerbate tuberculosis? Infect. Immun. *79*, 1407–1417.

Dillon, S.M., Lee, E.J., Donovan, A.M., Guo, K., Harper, M.S., Frank, D.N., McCarter, M.D., Santiago, M.L., and Wilson, C.C. (2016). Enhancement of HIV-1 infection and intestinal CD4+ T cell depletion ex vivo by gut microbes altered during chronic HIV-1 infection. Retrovirology *13*, 5.

Doitsh, G., Cavrois, M., Lassen, K.G., Zepeda, O., Yang, Z., Santiago, M.L., Hebbeler, A.M., and Greene, W.C. (2010). Abortive HIV infection mediates CD4 T cell depletion and inflammation in human lymphoid tissue. Cell *143*, 789–801.

Doitsh, G., Galloway, N.L., Geng, X., Yang, Z., Monroe, K.M., Zepeda, O., Hunt, P.W., Hatano, H., Sowinski, S., Muñoz-Arias, I., and Greene, W.C. (2014). Cell death by pyroptosis drives CD4 T-cell depletion in HIV-1 infection. Nature *505*, 509–514.

Dudek, T.E., and Allen, T.M. (2013). HIV-specific $CD8^+$ T-cell immunity in humanized bone marrow-liver-thymus mice. J. Infect. Dis. *208* (*Suppl 2*), S150–S154.

Dudek, T.E., No, D.C., Seung, E., Vrbanac, V.D., Fadda, L., Bhoumik, P., Boutwell, C.L., Power, K.A., Gladden, A.D., Battis, L., et al. (2012). Rapid evolution of HIV-1 to functional $CD8^+$ T cell responses in humanized BLT mice. Sci. Transl. Med. *4*, 143ra98.

Foreman, T.W., Mehra, S., LoBato, D.N., Malek, A., Alvarez, X., Golden, N.A., Bucşan, A.N., Didier, P.J., Doyle-Meyers, L.A., Russell-Lodrigue, K.E., et al. (2016). CD4+ T-cell-independent mechanisms suppress reactivation of latent tuberculosis in a macaque model of HIV coinfection. Proc. Natl. Acad. Sci. USA *113*, E5636–E5644.

Foreman, T.W., Mehra, S., Lackner, A.A., and Kaushal, D. (2017). Translational Research in the Nonhuman Primate Model of Tuberculosis. ILAR J. *58*, 151–159.

Gallegos, A.M., Pamer, E.G., and Glickman, M.S. (2008). Delayed protection by ESAT-6-specific effector CD4+ T cells after airborne M. tuberculosis infection. J. Exp. Med. *205*, 2359–2368.

Glushakova, S., Yi, Y., Grivel, J.C., Singh, A., Schols, D., De Clercq, E., Collman, R.G., and Margolis, L. (1999). Preferential coreceptor utilization and cytopathicity by dual-tropic HIV-1 in human lymphoid tissue ex vivo. J. Clin. Invest. *104*, R7–R11.

Graham, F.L., Smiley, J., Russell, W.C., and Nairn, R. (1977). Characteristics of a human cell line transformed by DNA from human adenovirus type 5. J. Gen. Virol. *36*, 59–74.

Grivel, J.C., Malkevitch, N., and Margolis, L. (2000a). Human immunodeficiency virus type 1 induces apoptosis in CD4(+) but not in CD8(+) T cells in ex vivo-infected human lymphoid tissue. J. Virol. *74*, 8077–8084.

Grivel, J.C., Penn, M.L., Eckstein, D.A., Schramm, B., Speck, R.F., Abbey, N.W., Herndier, B., Margolis, L., and Goldsmith, M.A. (2000b). Human immunodeficiency virus type 1 coreceptor preferences determine target T-cell depletion and cellular tropism in human lymphoid tissue. J. Virol. *74*, 5347–5351.

Grivel, J.C., Elliott, J., Lisco, A., Biancotto, A., Condack, C., Shattock, R.J., McGowan, I., Margolis, L., and Anton, P. (2007). HIV-1 pathogenesis differs in rectosigmoid and tonsillar tissues infected ex vivo with CCR5- and CXCR4-tropic HIV-1. AIDS *21*, 1263–1272.

Jekle, A., Keppler, O.T., De Clercq, E., Schols, D., Weinstein, M., and Goldsmith, M.A. (2003). In vivo evolution of human immunodeficiency virus type 1 toward increased pathogenicity through CXCR4-mediated killing of uninfected CD4 T cells. J. Virol. *77*, 5846–5854.

Kagina, B.M., Abel, B., Scriba, T.J., Hughes, E.J., Keyser, A., Soares, A., Gamieldien, H., Sidibana, M., Hatherill, M., Gelderbloem, S., et al.; other members of the South African Tuberculosis Vaccine Initiative (2010). Specific T cell frequency and cytokine expression profile do not correlate with protection against tuberculosis after bacillus Calmette-Guérin vaccination of newborns. Am. J. Respir. Crit. Care Med. *182*, 1073–1079.

Kaushal, D., Foreman, T.W., Gautam, U.S., Alvarez, X., Adekambi, T., Rangel-Moreno, J., Golden, N.A., Johnson, A.M., Phillips, B.L., Ahsan, M.H., et al. (2015). Mucosal vaccination with attenuated Mycobacterium tuberculosis induces strong central memory responses and protects against tuberculosis. Nat. Commun. *6*, 8533.

Kerkhoff, A.D., Barr, D.A., Schutz, C., Burton, R., Nicol, M.P., Lawn, S.D., and Meintjes, G. (2017). Disseminated tuberculosis among hospitalised HIV patients in South Africa: a common condition that can be rapidly diagnosed using urine-based assays. Sci. Rep. *7*, 10931.

Kløverpris, H.N., Kazer, S.W., Mjösberg, J., Mabuka, J.M., Wellmann, A., Ndhlovu, Z., Yadon, M.C., Nhamoyebonde, S., Muenchhoff, M., Simoni, Y., et al. (2016). Innate Lymphoid Cells Are Depleted Irreversibly during Acute HIV-1 Infection in the Absence of Viral Suppression. Immunity *44*, 391–405.

Knox, K.S., Vinton, C., Hage, C.A., Kohli, L.M., Twigg, H.L., 3rd, Klatt, N.R., Zwickl, B., Waltz, J., Goldman, M., Douek, D.C., and Brenchley, J.M. (2010). Reconstitution of CD4 T cells in bronchoalveolar lavage fluid after initiation of highly active antiretroviral therapy. J. Virol. *84*, 9010–9018.

Kumar, B.V., Ma, W., Miron, M., Granot, T., Guyer, R.S., Carpenter, D.J., Senda, T., Sun, X., Ho, S.H., Lerner, H., et al. (2017). Human Tissue-Resident Memory T Cells Are Defined by Core Transcriptional and Functional Signatures in Lymphoid and Mucosal Sites. Cell Rep. *20*, 2921–2934.

Kuroda, M.J., Sugimoto, C., Cai, Y., Merino, K.M., Mehra, S., Araínga, M., Roy, C.J., Midkiff, C.C., Alvarez, X., Didier, E.S., and Kaushal, D. (2018). High Turnover of Tissue Macrophages Contributes to Tuberculosis Reactivation in Simian Immunodeficiency Virus-Infected Rhesus Macaques. J. Infect. Dis. *217*, 1865–1874.

Kwon, D.S., Gregorio, G., Bitton, N., Hendrickson, W.A., and Littman, D.R. (2002). DC-SIGN-mediated internalization of HIV is required for trans-enhancement of T cell infection. Immunity *16*, 135–144.

Lawn, S.D., and Gupta-Wright, A. (2016). Detection of lipoarabinomannan (LAM) in urine is indicative of disseminated TB with renal involvement in patients living with HIV and advanced immunodeficiency: evidence and implications. Trans. R. Soc. Trop. Med. Hyg. *110*, 180–185.

Lawn, S.D., and Zumla, A.I. (2011). Tuberculosis. Lancet *378*, 57–72.

Lawn, S.D., Myer, L., Edwards, D., Bekker, L.G., and Wood, R. (2009). Short-term and long-term risk of tuberculosis associated with CD4 cell recovery during antiretroviral therapy in South Africa. AIDS *23*, 1717–1725.

Lee, J., Brehm, M.A., Greiner, D., Shultz, L.D., and Kornfeld, H. (2013). Engrafted human cells generate adaptive immune responses to Mycobacterium bovis BCG infection in humanized mice. BMC Immunol. *14*, 53.

Li, Q., Duan, L., Estes, J.D., Ma, Z.M., Rourke, T., Wang, Y., Reilly, C., Carlis, J., Miller, C.J., and Haase, A.T. (2005). Peak SIV replication in resting memory CD4+ T cells depletes gut lamina propria CD4+ T cells. Nature *434*, 1148–1152.

Lin, P.L., Myers, A., Smith, L., Bigbee, C., Bigbee, M., Fuhrman, C., Grieser, H., Chiosea, I., Voitenek, N.N., Capuano, S.V., et al. (2010). Tumor necrosis factor neutralization results in disseminated disease in acute and latent Mycobacterium tuberculosis infection with normal granuloma structure in a cynomolgus macaque model. Arthritis Rheum. *62*, 340–350.

Mahnke, Y.D., Brodie, T.M., Sallusto, F., Roederer, M., and Lugli, E. (2013). The who's who of T-cell differentiation: human memory T-cell subsets. Eur. J. Immunol. *43*, 2797–2809.

Mahomed, H., Hawkridge, T., Verver, S., Geiter, L., Hatherill, M., Abrahams, D.A., Ehrlich, R., Hanekom, W.A., and Hussey, G.D.; SATVI Adolescent Study Team (2011). Predictive factors for latent tuberculosis infection among adolescents in a high-burden area in South Africa. Int. J. Tuberc. Lung Dis. *15*, 331–336.

Mattapallil, J.J., Douek, D.C., Hill, B., Nishimura, Y., Martin, M., and Roederer, M. (2005). Massive infection and loss of memory CD4+ T cells in multiple tissues during acute SIV infection. Nature *434*, 1093–1097.

McMichael, A.J., Borrow, P., Tomaras, G.D., Goonetilleke, N., and Haynes, B.F. (2010). The immune response during acute HIV-1 infection: clues for vaccine development. Nat. Rev. Immunol. *10*, 11–23.

Mehra, S., Golden, N.A., Dutta, N.K., Midkiff, C.C., Alvarez, X., Doyle, L.A., Asher, M., Russell-Lodrigue, K., Monjure, C., Roy, C.J., et al. (2011). Reactivation of latent tuberculosis in rhesus macaques by coinfection with simian immunodeficiency virus. J. Med. Primatol. *40*, 233–243.

Mehra, S., Foreman, T.W., Didier, P.J., Ahsan, M.H., Hudock, T.A., Kissee, R., Golden, N.A., Gautam, U.S., Johnson, A.M., Alvarez, X., et al. (2015). The DosR Regulon Modulates Adaptive Immunity and Is Essential for Mycobacterium tuberculosis Persistence. Am. J. Respir. Crit. Care Med. *191*, 1185–1196.

Mogues, T., Goodrich, M.E., Ryan, L., LaCourse, R., and North, R.J. (2001). The relative importance of T cell subsets in immunity and immunopathology of airborne Mycobacterium tuberculosis infection in mice. J. Exp. Med. *193*, 271–280.

Monroe, K.M., Yang, Z., Johnson, J.R., Geng, X., Doitsh, G., Krogan, N.J., and Greene, W.C. (2014). IFI16 DNA sensor is required for death of lymphoid CD4 T cells abortively infected with HIV. Science *343*, 428–432.

Mörner, A., Björndal, A., Albert, J., Kewalramani, V.N., Littman, D.R., Inoue, R., Thorstensson, R., Fenyö, E.M., and Björling, E. (1999). Primary human immunodeficiency virus type 2 (HIV-2) isolates, like HIV-1 isolates, frequently use CCR5 but show promiscuity in coreceptor usage. J. Virol. *73*, 2343–2349.

Mothé, B.R., Lindestam Arlehamn, C.S., Dow, C., Dillon, M.B.C., Wiseman, R.W., Bohn, P., Karl, J., Golden, N.A., Gilpin, T., Foreman, T.W., et al. (2015). The TB-specific CD4(+) T cell immune repertoire in both cynomolgus and rhesus macaques largely overlap with humans. Tuberculosis (Edinb.) *95*, 722–735.

Murooka, T.T., Deruaz, M., Marangoni, F., Vrbanac, V.D., Seung, E., von Andrian, U.H., Tager, A.M., Luster, A.D., and Mempel, T.R. (2012). HIV-infected T cells are migratory vehicles for viral dissemination. Nature *490*, 283–287.

Mwale, A., Hummel, A., Mvaya, L., Kamng'ona, R., Chimbayo, E., Phiri, J., Malamba, R., Kankwatira, A., Mwandumba, H.C., and Jambo, K.C. (2018). B cell, CD8+ T cell and gamma delta T cell infiltration alters alveolar immune cell homeostasis in HIV-infected Malawian adults. Wellcome Open Res. *2*, 105.

Neff, C.P., Chain, J.L., MaWhinney, S., Martin, A.K., Linderman, D.J., Flores, S.C., Campbell, T.B., Palmer, B.E., and Fontenot, A.P. (2015). Lymphocytic alveolitis is associated with the accumulation of functionally impaired HIV-specific T cells in the lung of antiretroviral therapy-naive subjects. Am. J. Respir. Crit. Care Med. *191*, 464–473.

Okoye, A.A., and Picker, L.J. (2013). CD4(+) T-cell depletion in HIV infection: mechanisms of immunological failure. Immunol. Rev. *254*, 54–64.

Penn, M.L., Grivel, J.C., Schramm, B., Goldsmith, M.A., and Margolis, L. (1999). CXCR4 utilization is sufficient to trigger CD4+ T cell depletion in HIV-1-infected human lymphoid tissue. Proc. Natl. Acad. Sci. USA *96*, 663–668.

Purwar, R., Campbell, J., Murphy, G., Richards, W.G., Clark, R.A., and Kupper, T.S. (2011). Resident memory T cells (T(RM)) are abundant in human lung: diversity, function, and antigen specificity. PLoS ONE *6*, e16245.

Sakai, S., Kauffman, K.D., Schenkel, J.M., McBerry, C.C., Mayer-Barber, K.D., Masopust, D., and Barber, D.L. (2014). Cutting edge: control of Mycobacterium tuberculosis infection by a subset of lung parenchyma-homing CD4 T cells. J. Immunol. *192*, 2965–2969.

Sallin, M.A., Sakai, S., Kauffman, K.D., Young, H.A., Zhu, J., and Barber, D.L. (2017). Th1 Differentiation Drives the Accumulation of Intravascular, Non-protective CD4 T Cells during Tuberculosis. Cell Rep. *18*, 3091–3104.

Sonnenberg, P., Glynn, J.R., Fielding, K., Murray, J., Godfrey-Faussett, P., and Shearer, S. (2005). How soon after infection with HIV does the risk of tuberculosis start to increase? A retrospective cohort study in South African gold miners. J. Infect. Dis. *191*, 150–158.

Steele, A.K., Lee, E.J., Manuzak, J.A., Dillon, S.M., Beckham, J.D., McCarter, M.D., Santiago, M.L., and Wilson, C.C. (2014). Microbial exposure alters HIV-1-induced mucosal CD4+ T cell death pathways Ex vivo. Retrovirology *11*, 14.

Veazey, R.S., Tham, I.C., Mansfield, K.G., DeMaria, M., Forand, A.E., Shvetz, D.E., Chalifoux, L.V., Sehgal, P.K., and Lackner, A.A. (2000). Identifying the target cell in primary simian immunodeficiency virus (SIV) infection: highly activated memory CD4(+) T cells are rapidly eliminated in early SIV infection in vivo. J. Virol. *74*, 57–64.

Verhoeven, D., George, M.D., Hu, W., Dang, A.T., Smit-McBride, Z., Reay, E., Macal, M., Fenton, A., Sankaran-Walters, S., and Dandekar, S. (2014). Enhanced innate antiviral gene expression, IFN-α, and cytolytic responses are predictive of mucosal immune recovery during simian immunodeficiency virus infection. J. Immunol. *192*, 3308–3318.

Wong, E.B., Akilimali, N.A., Govender, P., Sullivan, Z.A., Cosgrove, C., Pillay, M., Lewinsohn, D.M., Bishai, W.R., Walker, B.D., Ndung'u, T., et al. (2013). Low levels of peripheral CD161++CD8+ mucosal associated invariant T (MAIT) cells are found in HIV and HIV/TB co-infection. PLoS ONE *8*, e83474.

Zens, K.D., Chen, J.K., and Farber, D.L. (2016). Vaccine-generated lung tissue-resident memory T cells provide heterosubtypic protection to influenza infection. JCI Insight *1*, e85832.

STAR★METHODS

KEY RESOURCES TABLE

REAGENT or RESOURCE	SOURCE	IDENTIFIER
Antibodies		
CD3	BD Biosciences	Cat# 562280; RRID: AB_11153674
CD4	BD Biosciences	Cat# 557922; RRID: AB_396943
CD8	Biolegend	Cat# 300925; RRID: AB_10612924
CD45	BD Biosciences	Cat# 560777; RRID: AB_1937324
TCRa/b	Biolegend	Cat# 306710; RRID: AB_314648
CD103	Biolegend	Cat# 350212; RRID: AB_2561599
CD25	BD Biosciences	Cat# 563159; RRID: AB_2738037
CD69	BD Biosciences	Cat# 555530; RRID: AB_395915
CD62L	Biolegend	Cat# 304810; RRID: AB_314470
CXCR3	Biolegend	Cat# 353728; RRID: AB_2563157
CD45RO	BD Biosciences	Cat# 560607; RRID: AB_1727500
CD49a	Biolegend	Cat# 328304; RRID: AB_1236407
CD11a	BD Biosciences	Cat# 563937
CD4	Biolegend	Cat# 300555; AB_2564390
CCR5	BD Biosciences	Cat# 300555; RRID: AB_2564390
HIV-1p24	Beckman Coulter	Cat# 6604667; RRID: AB_1575989
CD4	BD Biosciences	Cat# 550631; RRID: AB_393791
CD8	BD Biosciences	Cat# 555369; RRID: AB_398595
CD3	BD Biosciences	Cat# 557917; RRID: AB_396938
CD28	BD Biosciences	Cat# 555726; RRID: AB_396069
CD95	BD Biosciences	Cat# 555671; RRID: AB_396024
anti human CD4	Abcam	Cat# ab67001; RRID: AB_1139906
Bacterial and Virus Strains		
HIV-1 NL4-3 CCR5-tropic GFP	Murooka et al., 2012	N/A
HIV-1 NL4-3 CXCR4-tropic GFP	Murooka et al., 2012	N/A
HIV-1 JRCSF	Boutwell et al., 2009	N/A
SIVmac239	Foreman et al., 2016	N/A
Mycobacterium tuberculosis CDC1551	Foreman et al., 2016	N/A
Biological Samples		
Human PBMCs	MGH blood donor center	N/A
Tonsil tissue	MGH Eye and Ear Infirmary	N/A
Lung tissue	MGH Pathology lab	N/A
Chemicals, Peptides, and Recombinant Proteins		
Histopaque 1077	Sigma Aldrich	Cat# 10771
CD45 enrichment kit	StemCell	Cat# 18529
Live/Dead fixable Blue dead cell stain kit	ThermoFisher Scientific	Cat# L23105
HIV-1 p24 ELISA	PerkinElmer	Cat# NEK050B001KT
Maraviroc	Sigma Aldrich	Cat# PZ0002
AMD3100	Sigma Aldrich	Cat# A5602
Zidovudine (AZT)	Sigma Aldrich	Cat# PHR1292
Efavirenz	Sigma Aldrich	Cat# SML0536
Raltegravir	Santa Cruz Biotechnology	Cat# CAS 871038-72-1
Darunavir	Sigma Aldrich	Cat# SML0937

(*Continued on next page*)

Continued

REAGENT or RESOURCE	SOURCE	IDENTIFIER
Z-VAD-FMK	R&D systems	Cat# FMK001
Z-DEVD-FMK	R&D systems	Cat# FMK004
Z-WEHD-FMK	R&D systems	Cat# FMK002
Annexin-V buffer	BD Biosciences	Cat# 556454
Annexin-V APC	BD Biosciences	Cat# 550474
Fix & Perm buffer	Life technology	Cat# GAS003
progesteron (Depo-provera)	Pfizer	N/A
Critical Commercial Assays		
RNAeasy microkit	QIAGEN	Cat# 74004
QuantiFAST SYBR green RT-PCR kit	QIAGEN	Cat# 204154
Experimental Models: Cell Lines		
GHOST cell line	NIH AIDS Research & Reference Reagent Program	N/A
HEK293 T cell line	NIH AIDS Research & Reference Reagent Program	N/A
Experimental Models: Organisms/Strains		
Humanized mouse	MGH Human Immune system core	N/A
Non-human primates	Tulane National Primate Research Center	N/A
Oligonucleotides		
HIV-1 gag forward	AGTGGGGGGACATCAAGCAGCCATGCAAAT	Boutwell et al., 2013
HIV-1 gag reverse	TGCTATGTCACTTCCCCTTGGTTCTCT	Boutwell et al., 2013
Software and Algorithms		
GraphPad Prism7	Graphpad software	N/A
Flow Jo Vx0.7	FlowJo, LLC	N/A

CONTACT FOR REAGENT AND RESOURCE SHARING

Further information for reagents and resources can be addressed to and will be fulfilled by the Lead Contact, Dr. Björn Corleis (bcorleis@mgh.harvard.edu).

EXPERIMENTAL MODEL AND SUBJECT DETAILS

Human subjects

All work involving material from human subjects was approved by the Institutional Review Board (IRB) at Massachusetts General Hospital (MGH). For PBMCs, cells were isolated from buffy coats of anonymous healthy blood donors obtained from the MGH blood donor center (Boston, MA) after approval by the Partners Human Research Committee under protocol 2005P001218. Tonsil and lung tissue was received as excess tissue from the Pathology Departments of MGH and the operating room at the Massachusetts Eye and Ear Infirmary (Table S1). Sex, age and post-operation diagnosis of patient samples are summarized in Table S1. The use of surgical excess tissue was approved by the Partners Human Research Committee under the approved protocol # 2010P000632. Sample size was based on feasibility and availability of human excess tissue collections. Donor matched controls were used for all experimental conditions.

Humanized mouse

Humanized mice were purchased from the MGH Human Immune System Mouse Core (Boston, USA). All humanized mouse work was approved by the Institutional Animal Care and Use Committee (IACUC) at MGH under the protocol # 2009N000136 adhering to the United States Animal Welfare Act and the Animal Welfare Regulations. Humanized mice were all female and 6-8 weeks of age during engraftment of human tissue.

Non-human primates

Non-human primate experiments and procedures were approved by the Institutional Animal Care and Use Committee of Tulane University, New Orleans, LA, and were performed in accordance with NIH guidelines and under the protocols # PO295, PO295R, PO247R, PO065, PO324 and P0095. For this study, we analyzed 26 specific pathogen-free, retrovirus-free, mycobacteria-naive,

male, adult Indian rhesus macaques (NHPs) between the ages of 3-12 years that were bred and housed at the Tulane National Primate Research Center (TNPRC). NHPs were pair-housed during the duration of the study. Additional analysis has been performed using experimental data originally generated in a prior study of SIV infected animals (Foreman et al., 2016), as well as additional animals (Table S2).

Cell lines

The human female kidney cell line, HEK293 (Graham et al., 1977), first isolated from primary embryonic kidney tissue and transformed by sheared human adenovirus type 5 (Ad5 DNA) and the human osteosarcoma cell line, GHOST CXCR4+CCR5+ (Mörner et al., 1999), first isolated from human osteosarcoma cells of unknown sex which were stably transduced with a MV7neo-T4 vector, the MLV-CCR5 BABE-puro vector, the MX-CCR4 and MX-CCR5 vector and cotransfected with HIV-2 LTR-GFP, were obtained from the NIH AIDS Reagent Program. Cells were maintained in DMSO (GIBCO) supplemented with 10% (v/v) FCS (Sigma), 2 mM Glutamine (Corning), 100 I.U./ml penicillin (Corning) and 100 I.U./ml streptomycin (Corning). GHOST CXCR4+CCR5+ cell cultures were additionally supplemented with 100 μg/ml hygromycin (Corning) and 1 μg/ml puromycin (Corning).

METHOD DETAILS

Human blood and tissue samples

PBMCs were separated by centrifugation on a histopaque gradient and used fresh. In all cases, we received macroscopically healthy disease-free tissue sections that were further examined by a pathologist in frozen sections and found to be histologically normal. Human tissue was processed fresh and at 4°C. Blood contamination of tissues was minimized by exclusion of tissue sections which demonstrated significant blood contamination by gross pathological examination. Further, tissues were washed 3 times with FACS buffer (PBS+1%FCS+5mM EDTA). Fresh single cell suspensions from lung and tonsil tissue were made by mechanically disrupting dissected tissue using a cell strainer and a 10 mL syringe plunger. Frequency of CD45+ leukocytes was high in tonsil (> 98%), but low in whole lung single cell suspension (1%–2%). Therefore, lung CD45+ leukocytes were enriched from whole lung tissue single suspension using a CD45 enrichment kit (Stemcell) for magnetic-activated cell sorting (MACS) according to the manufacturer's instructions. Blood or tissue single cell suspensions were collected in R10 (RPMI (Sigma), 10% (v/v) FCS (Sigma), 2 mM Glutamine (Corning), 100 I.U./ml penicillin (Corning) and 100 I.U./ml streptomycin (Corning)) and used for further studies.

HIV-1 *in vitro* infection assay

HIV-1 NL4-3 CCR5-tropic, CXCR4-tropic GFP or JR-CSF HIV-1 virus was used for all *in vitro* experiments. The plasmids were kindly provided by Thomas Murooka and Thorsten Mempel (Murooka et al., 2012). For production of HIV-1, viral plasmids were transfected together with FuGENE-6 (Polysience) into HEK293 cells and incubated overnight at 37°C and 5% CO_2. Cell culture supernatants were removed and replaced with fresh media for 48h under the same culture conditions. Cell culture supernatants were harvested and centrifuged at 500xg for 10 min at 4°C. Supernatants were aliquoted and frozen down at-80°C until further usage. Mock supernatants were prepared under the same protocol without the addition of viral plasmids during the transfection steps. Titer of HIV-1 NL4-3 infectious particles (i.p.)/ml was determined by infection of CD4, CCR5, and CXCR4 expressing GHOST cells (NIH AIDS Research & Reference Reagent Program) (Kwon et al., 2002). Additionally, HIV-1 p24 protein levels were determined by ELISA (PerkinElmer) following the manufacturer's instructions. A viral stock with a titer of $2x10^6$ i.p./ml ($1.9x10^6$ pg/ml $p24^{gag}$ protein) was used for all experiments. $0.5x10^6$ human leukocytes from blood, tonsil or lung cells were mixed with $0.1x10^6$ infectious viral particles (MOI = 0.2 equivalent to 95ng $p24^{gag}$) in a 96 well V-bottomed polystyrene plate in a total volume of 100 μL and kept at 4°C. Where indicated, cells were pre-incubated with anti-retroviral drugs or chemical inhibitors for 30 min at 37°C before infection and were consistently present throughout the experiment. Leukocyte/HIV cultures were spin-infected for 90 min at 4°C and 800 x g and were then incubated at 37°C for 12 hr. Supernatants containing cell free virus were taken off and replaced with fresh media. Cells were harvested after 96 hr to analyze the number of live CD4+ T cells and the percentage of virus producing GFP+ cells. ART drugs were all purchased from Sigma-Aldrich and used at the following effective and nontoxic concentrations: 40 μM maraviroc (MVA), 250 nM AMD3100 (AMD), 10 μM Zidovudine (AZT), 100 nM Efavirenz (EFV), 12.5 nM Raltegravir (RAL), and 25 nM Darunavir (DRV). For inhibition of caspase activity, the following chemical inhibitors from R&D systems were used at a concentration of 10 μM: pan-caspase inhibitor Z-VAD-FMK, caspase 3 inhibitor Z-DEVD-FMK, and caspase 1 inhibitor Z-WEHD-FMK.

Flow cytometry

Human cells from *ex vivo* or *in vivo* experiments were resuspended in FACS buffer (PBS+1%FCS+5mM EDTA) and centrifuged for 5 min at 1500 x g at 4°C. Cell pellets were stained with antibodies against cell surface antigens and with blue or green viability dye (Invitrogen fixable viability dye) to exclude dead cells from analysis, for 20 min at room temperature (RT). Details for all specific and titrated monoclonal antibodies are listed in the resource table. For analysis of T cells in human and humanized mouse samples, cell pellets were stained with anti CD45 (HI30), CD3 (UCHT1), CD4 (RPA-T4) and CD8 (HIT8a). Tissue resident CD4+ T cells were assessed by incubating cells with antibodies binding to TCRαβ (IP26), CD103 (Ber-ACT8), CD25 (2A3), CD69 (FN50), CD62L (DREG-56), CXCR3 (G025H7), CD45RO (UCHL1), and CD11a (HI111). HIV-1 co-receptor expression was analyzed using an antibody detecting human CCR5 (2D7/CCR5). Memory CD4+ T cells in NHPs were defined using anti CD95 (DX2) and anti CD28 (CD28.2), with

effector memory (T_{EM}) CD4+ T cells CD95+CD28- and central memory (T_{CM}) CD4+ T cells CD95+CD28+. For detection of apoptotic cells, all washing steps were performed in Annexin-V washing buffer (BD Bioscience), before and after staining with Annexin V-APC (BD Bioscience) for 10 min at RT. Cells were stained for intracellular HIV-1 gag p24 by incubating cells with fixation/permeabilization buffer A (Invitrogen) for 20 min at RT, followed by a washing step with PBS and addition of perm/fix buffer B (Invitrogen) for 15 min at RT. HIV-1 infected cells were stained with an antibody binding HIV p24 (KC57) and incubated for 30 min at 4°C. Cells were fixed with 2% PFA before running on a LSR Fortessa flow cytometer (BD Biosciences) within 4 hr, or immediately in case of Annexin-V stained samples. Flow data were analyzed with FlowJo (TreeStar). Countbright beads (Invitrogen) were added to calculate total CD4+ T cells in lung, tonsil and PBMCs samples following the manufacturer's instructions.

HIV-1 *in vivo* humanized mouse infection

JR-CSF HIV-1, was purchased from the virology core at the Ragon Institute of MGH, MIT and Harvard and was used for experiments in the humanized mouse as described (Boutwell et al., 2009). Bone marrow/Liver/Thymus (BLT) humanized were purchased from the MGH Human Immune System Mouse Core (HISMC, Boston, USA) as described in the ethical statement. Six to 8 weeks old female BLT-NOD-scid IL2R$\gamma-/-$ (NSG) mice (The Jackson Laboratory) were housed in a pathogen-free facility at MGH, and reconstituted with human tissue by the HISMC as described previously (Deruaz et al., 2017). BLT-NSG mice were obtained after successful human immune cell reconstitution (> 40% of lymphocytes were human CD45+ of which > 30% of were CD3+ and a minimum of > 200 CD4+ T cells/uL) 13-18 weeks post-surgery. A total of 34 humanized BLT-NSG mice from 2 different batches generated with different donor tissues were used. One mouse was excluded from the analysis due to the development of severe graft versus host disease (GvHD) during the experiment. Mice were infected with atraumatic intravaginal (IVAG) application of $0.5x10^5$ $TCID_{50}$ $HIV\text{-}1_{JRCSF}$ in 10-20 μl PBS as previously described (Deruaz et al., 2017). Mice were treated 5 days prior to challenge with a subcutaneous injection of 200 μg of progesterone (Depo-Provera medroxyprogesterone acetate, Pfizer) in a total volume of 100 μl of PBS. HIV-1 JRCSF infected mice and uninfected control mice were euthanized 4 or 7 weeks post infection. Intravascular staining of human CD45+ cells was adopted from (Anderson et al., 2014). For this, 3 μg of anti-human CD45 v500 (clone HI100, Biolegend) were injected i.v. in a total volume of 200 μL PBS. 3 min after antibody injection, the animals were euthanized. The method allows to distinguish lung vascular from interstitial and alveolar CD4+ T cells. Since the number of interstitial CD4+ T cells exceeds the number alveolar CD4+ T cells, we defined CD45iv- cells as interstitial CD4+ T cells. The following samples were collected: BAL, lung, spleen, and blood. BAL was obtained by injection and recovery of 1 mL PBS through the trachea. Single cell suspensions from spleen and lung tissues were obtained as described for human surgical tissue. The post-caval lobe of the lung was reserved for immunohistochemistry and placed in 10% formalin. The right middle lobe was stored at −80°C in RNAlater and reserved for HIV-1 RNA extraction. Similar proportions of spleen tissue were processed the same way.

HIV-1 gag RNA reverse transcriptase quantitative PCR (RT-qPCR)

RNA was extracted from homogenized tissue and sorted cell populations using the RNAeasy kit (QIAGEN) following the manufacturer's protocol. RNA was resuspended in RNase free water and stored in aliquots at −80°C. RT-qPCR was performed using HIV-1 gag-specific primers (SK145 forward, AGTGGGGGGACATCAAGCAGCATGCAAAT and SK431 reverse, TGCTATGTC ACTTCCCCTTGGTTCTCT), quantified using the QuantiTect SYBR green RT-PCR kit (QIAGEN) according to the manufacturer's instructions and using a Roche 384 well plate Lightcycler 480-II (Roche). Concentrations of HIV-1 gag RNA were calculated from a linear gag HIV-1 HxB2 standard kindly provided by Dr. Christian Boutwell (Boutwell et al., 2009). Results were normalized for tissue weight (in ng) or total cell numbers for tissue samples and sorted cells, respectively.

Immunohistochemistry

Formalin fixed, paraffin embedded tissue from lung and spleen samples of HIV-1 infected and uninfected mice were cut in 4 μm sections. Antigen retrieval was carried out in a Decloaking Chamber (BioCare Medical), in citrate buffer pH 6 (Invitrogen). Sections were incubated with anti-HIV-1 p24 (1:50; clone KC57 Beckman Coulter) or anti-human CD4 (1:50; clone 1F6 Abcam) antibody overnight at 4°C. Slides were washed five times in Tris buffered saline with 0.05% Tween-20 (TBST). Secondary anti-mouse HRP conjugated antibody (Dako) was applied for 1 hr at RT. After another five washes with TBST, staining was visualized using DAB substrate (Dako). Tissue samples were counterstained with Harris Modified Hematoxylin (Sigma). Whole tissue slide sections were scanned with an Olympus TissueFAXS whole slide scanning system and the number of p24+ or CD4+ cells were quantified using HistoQuest software (TissueGnostics) and by taking the average of 2 consecutive tissue sections from per sample. Background was subtracted for each sample by staining 2 consecutive tissue sections without the addition of the secondary antibody. The average number of unspecific stained cells from 2 slides were subtracted from the average number of CD4+ or p24+ cells.

Mycobacterium tuberculosis / SIV infection in nonhuman primates

We retrospectively analyzed and compared CD4+ T cells in the lung and blood of SIV uninfected versus SIV infected animals (Table S2). The experiment and data collection were performed as following and described previously (Foreman et al., 2016). All animals were aerosol exposed to a low dose (~10-25 CFU implanted) of *Mtb* CDC1551 and after maintenance of LTBI for up to 9 weeks, a subset of 15 of the macaques was co-infected with 300 TCID50 of SIVmac239 administered intravenously, as described previously (Foreman et al., 2016, 2017; Kuroda et al., 2018; Mehra et al., 2011). Group distributions were assigned based on clinical outcomes

during *Mtb* and *Mtb*/SIV co-infection. LTBI in NHPs was defined as asymptomatic without clinical signs for the duration of the study and as described previously (Mothé et al., 2015). Criteria for active tuberculosis (reactivation) during the study were described before (Foreman et al., 2016) and included *Mtb* culture positive BAL, chest X-ray, body temperature, weight, and maintenance of a CRP value above 3 mg/mL or more for 3 consecutive weeks. Early animal euthanasia due to discomfort, were performed as previously described (Foreman et al., 2016). Clinical assessments and lung pathology post-necropsy (% lung involvement) were performed by veterinary clinicians in a blinded fashion and previously described (Foreman et al., 2016; Kaushal et al., 2015). BAL samples were obtained by bronchoscopy before necropsy, and total cell numbers and T cell phenotypes were assessed in 1/20 of the recovered BAL volume by flow cytometry. Necropsy was performed 20-22 weeks post-*Mtb* infection. Lung, spleen, bronchial lymph nodes (Br LN), kidney and liver tissues were collected and processed with bacterial load analyzed by colony forming unit assay (CFU) as described (Foreman et al., 2016; Mehra et al., 2011, 2015). CD4+ and CD8+ T cell numbers were analyzed in $1x10^6$ total tissue cells or 100 μL of whole EDTA blood by flow cytometry using anti-human or anti-NHPs antibodies against CD4 (L200), CD8 (RPA-T8), CD3 (SP34-2), CD28 (CD28.2), CD95 (DX2).

QUANTIFICATION AND STATISTICAL ANALYSIS

Statistical details of experiments can be found in each figure legend. Nonparametric tests were used to compare medians between groups. The Mann-Whitney test was used for 2 groups and the Kruskal-Wallis test followed by Dunn's multiple comparison post test was used for > 2 groups. Wilcoxon signed rank was used to compare continuous data between two time points. Spearman's correlation coefficients were used to examine associations between variables. Differences were considered significant at $p < 0.05$. Prism 7 (Graphpad) was used for all analyses.

Cell Reports, Volume *26*

Supplemental Information

HIV-1 and SIV Infection Are Associated with Early Loss of Lung Interstitial CD4+ T Cells and Dissemination of Pulmonary Tuberculosis

Björn Corleis, Allison N. Bucsan, Maud Deruaz, Vladimir D. Vrbanac, Antonella C. Lisanti-Park, Samantha J. Gates, Alice H. Linder, Jeffrey M. Paer, Gregory S. Olson, Brittany A. Bowman, Abigail E. Schiff, Benjamin D. Medoff, Andrew M. Tager, Andrew D. Luster, Shabaana A. Khader, Deepak Kaushal, and Douglas S. Kwon

Supplemental Information

Figure S1

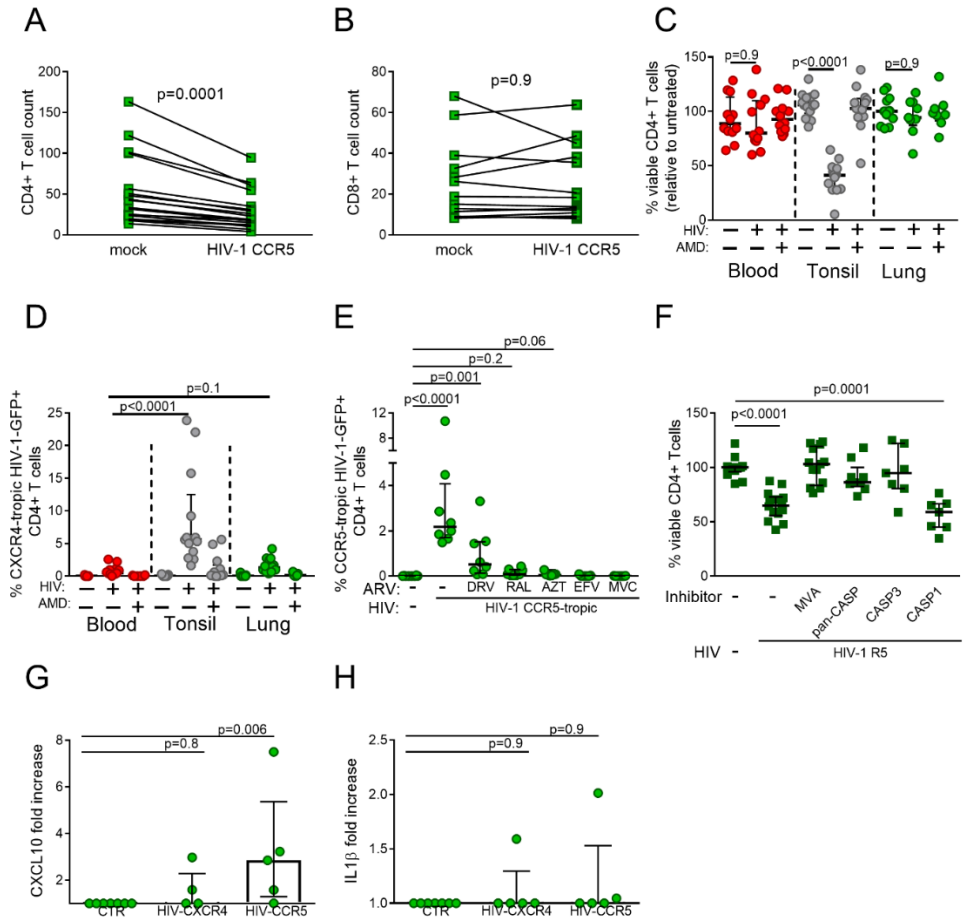

Figure S1. Depletion of lung CD4+ T cells is associated with productively infected cells. Related to Figure 1. Isolation of cells and infection with HIV-1 was performed as described in Figure 1. (A and B) Total cell counts of (A) CD4+ and (B) CD8+ T cells was analyzed by flow cytometry in paired samples mock infected or infected with CCR5-tropic HIV-1. Blood, tonsil or lung cells were infected with CXCR4-tropic NL4-3 GFP HIV-1, mock infected or left untreated. Where indicated, cells were incubated with the CXCR4 antagonist plerixafor (AMD3100) before infection. (C). Percentage of viable CD4+ T cells (D) was determined relative to untreated cells by flow cytometry. (E) Analysis of CCR5-tropic HIV-1 GFP+ CD4+ T cells from samples analyzed for viable CD4+ T cells in Figure 1F. (F) Lung cells were pre-incubated with the CCR5 antagonist maraviroc [MVA], the pan-caspase inhibitor Z-VAD-FMK [pan-CASP], the caspase 3 inhibitor Z-DEVD-FMK [CASP3], or the caspase-1 inhibitor Z-WEHD-FMK [CASP1] before infection with HIV-1 as described in Figure 1, and CD4+ T cells were analyzed for viabilty by flow cytometry. (G and H) CXCL10 and IL1 protein level in cell culture supernatants were analyzed using the Luminex multiplex platform. p-value was measured by (A and B) Wilcoxon test or (C-H) Kruskal Wallis and Dunn's multiple comparisons. Scatter plots are labeled with median and interquartile range.

Figure S2

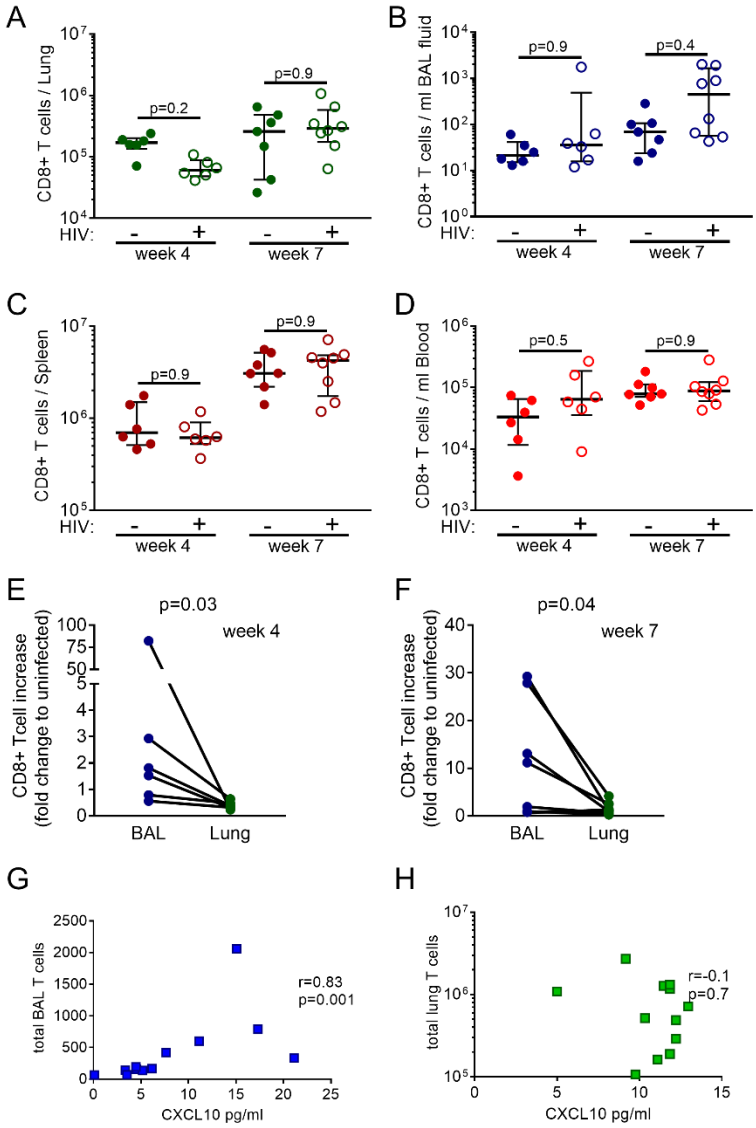

Figure S2. CD8+ T cells are increased in BAL compared to lung tissue. Related to Figure 2. The same batch of mice described in Figure 2 was analyzed for CD8+ T cell numbers in (A) lung, (B) BAL, (C) spleen and (D) blood by flow cytometry. (E and F) CD8+ T cell increases in paired BAL and lung samples were analyzed as fold increase compared to the median CD8+ T cell count of uninfected animals at (E) 4 weeks or (F) 7 weeks post infection. The CD8 T cell recruiting chemokine CXCL10 was measured by Luminex in BAL fluid 9G) or supernatants from lung tissue single cell suspensions (H) in samples obtained 4 weeks post infection. p-value was measured by (A-D) Kruskal Wallis and Dunn's multiple comparisons test, (E and F) Wilcoxon test or (G and H) by Spearman r test. Scatter plots are labeled with median and interquartile range.

Figure S3

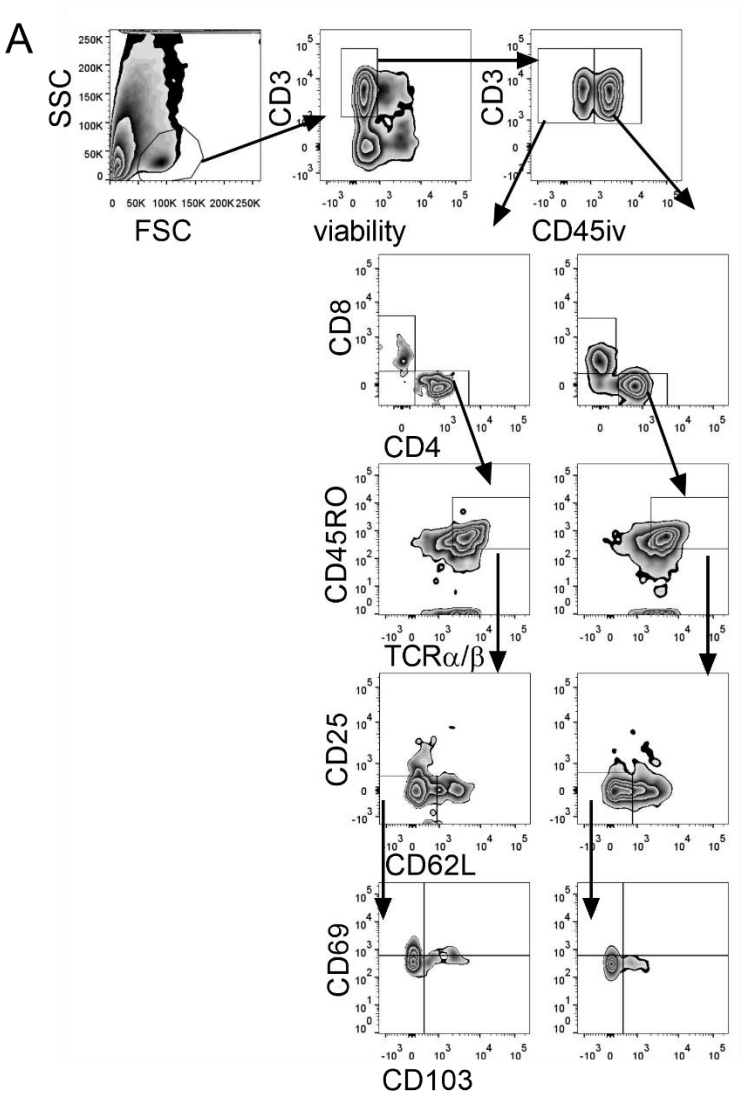

Figure S3. Gating strategy for CD4+ T_{RM}-like cells by flow cytometry. Related to Figure 4. Representative gating strategy for T_{RM}-like cells in humanized mouse lung tissue. Gating started on positive selection of the lymphocyte population by SSC/FSC. Viable T cells were selected by gating on CD3+ fixable cell death dye- lymphocytes. Lung parenchyma CD4+ T cells were separated from lung vascular CD4+ T cells by anti-human CD45 *in vivo* labeling of circulating cells 3 min before sacrificing the humanized mice. This resulted in CD3+ populations which were either CD45iv- or CD45iv+. Next, CD45iv- and CD45iv+ were separated into CD4+ and CD8+ T cells. CD4+ T cells were positively selected for memory cells by CD45RO+ and innate-like γδ T cells were excluded by positive selection of TCRαβ expressing CD45RO+ CD4+ T cells. Central memory and activated CD4+ T cells were excluded by negative selection of CD62L- and CD25- CD45RO+ CD4+ T cells, respectively. CD4+ T_{RM} cells were defined as viable CD3+ CD4+ CD45RO+ TCRαβ+ CD25- CD62L-CD69+. Representative images for all analyzed compartments are shown.

Figure S4

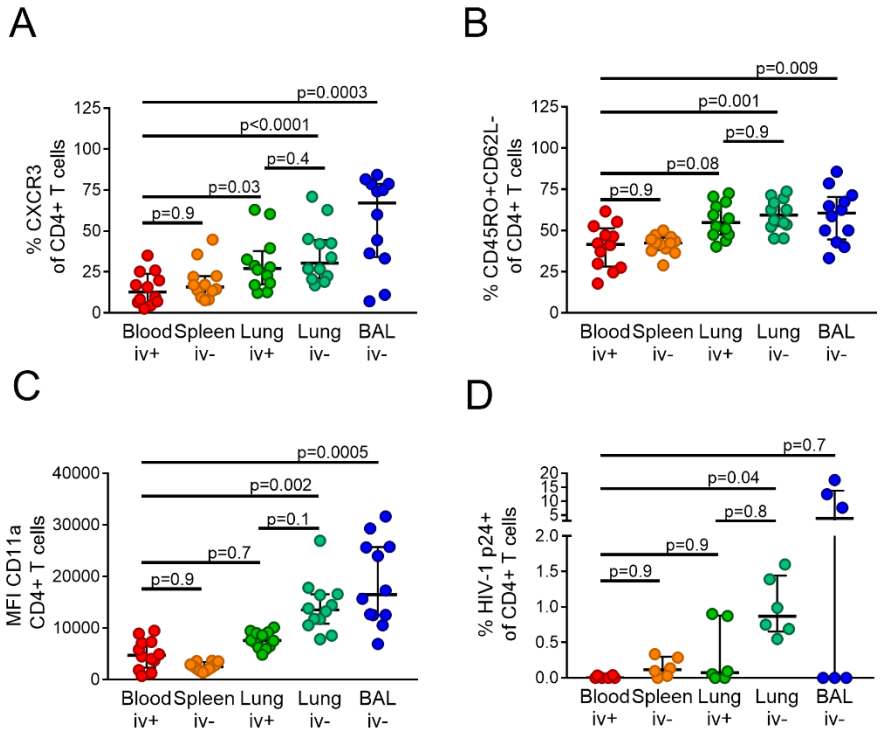

Figure S4. Characterization of lung interstitium CD4+ T cells by flow cytometry. Related to Figure 4. HIV-1 infected (4 weeks) humanized mice (n=6) or uninfected control mice (n=12) were iv injected with an anti-human CD45 antibody 3 mins prior to sacrifice. CD45iv negative and positive CD4+ T cells were analyzed in lung, BAL, spleen and blood by flow cytometry (see Figure S3 for gating strategy). The T_{RM} phenotype of CD45iv labeled (lung iv+) or unlabeled CD45iv (lung iv-) CD4+ T cells was further characterized by flow cytometry. Percentage of all CD4+ T cells with (A) surface expression of CXCR3+ and (B) expression memory CD4+ T cell markers (CD45RO+CD62L-) was determined. (C) The median fluorescence intensity (MFI) of CD11a was analyzed. CD4+ T cells were gated on viable CD4+ TCRα/β+CD45RO+CD62L-CD25- T cells. (D) *In vivo* productively infected CD4+ T cells were analyzed by intracellular staining for HIV-1 p24+ and gating on all viable CD4+ T cells. p-value was measured by Kruskal Wallis and Dunn's multiple comparisons test. Scatter plots are labeled with median and interquartile range.

Figure S5

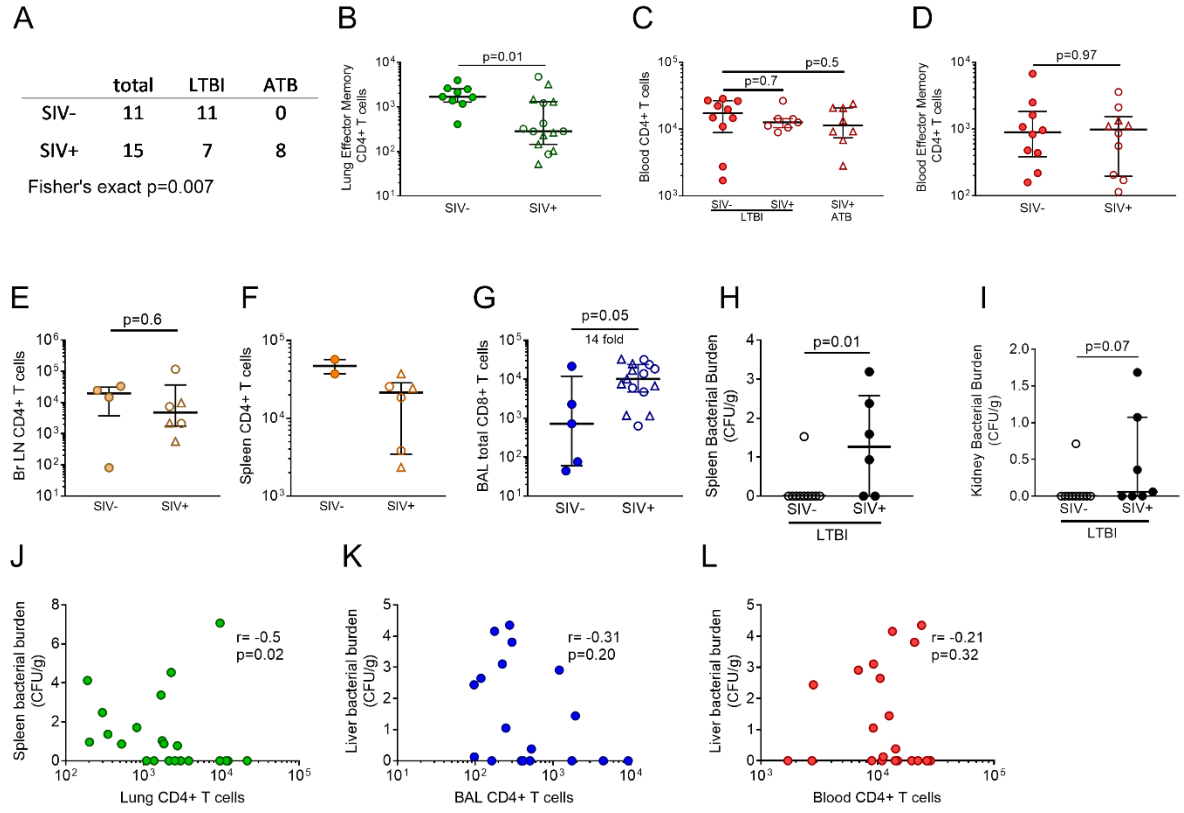

Figure S5. SIV/*Mtb* co-infection leads to increased development of active and disseminated tuberculosis. Related to Figure 5. (A) 26 NHPs were infected with *Mtb* resulting in LTBI. After 9 weeks 15 NHPs were co-infected with SIV. 8 *Mtb*/SIV co-infected and 0 *Mtb* infected animals progressed to ATB. (B-F) CD4+ T cell loss in different compartments was analyzed in NHPs with LTBI or ATB by flow cytometry. (B and D) Cells were additionally stained with CD28 and CD95 and effector memory CD4+ T cells were defined as CD28-CD95+ (G) CD8+ T cells in BAL were analyzed in *Mtb*/SIV co-infected and *Mtb* infected NHPs by flow cytometry. Mtb burden was determined in (H) spleen and (I) kidney by CFU. Correlation of (J) spleen *Mtb* bacterial burden versus lung parenchymal CD4+ T cells and (K) liver bacterial burden versus BAL CD4+ T cells or (L) blood CD4+ T cells. p-value was measured by (A) Fisher's exact, (B and D-I) Mann-Whitney U-test, (C) Kruskal Wallis with Dunn's multiple comparisons test, or (J-L) by Spearman r test. Scatter plots are labeled with median and interquartile range.

Table S1. Demographics and post-operative diagnosis of patient samples used for excess tissue experiments. Related to Figure 1.

Sample ID	Collection Date	Sample Type	Age	Sex	Post-Op Diagnosis
LU1631	11/23/2015	Lung	70	Male	Lung hamartoma
LU1632	12/2/2015	Lung	68	Female	Left upper lobe adenocarcinoma
LU1637	12/11/2015	Lung	77	Female	Squamous cell carcinoma of the lung
LU1638	12/14/2015	Lung	52	Male	Unknown source of hemoptysis
LU1639	12/16/2015	Lung	37	Male	Carcinoid tumor of right lower lobe
LU1643	1/4/2016	Lung	60	Female	Adenocarcinoma of the lung
LU1654	2/1/2016	Lung	65	Female	Adenocarcinoma of the lung
LU1660	2/11/2016	Lung	65	Male	Left local lobe adenocarcinoma
LU1676	3/4/2016	Lung	76	Male	Left upper lobe lung cancer
LU1695	3/29/2016	Lung	65	Female	Left upper lobe lung cancer
LU1703	4/27/2016	Lung	43	Female	Right lower lobe adenocarcinoma
LU1705	5/2/2016	Lung	75	Female	Lung carcinoma
LU1708	5/16/2016	Lung	65	Male	Adenocarcinoma, left lower lobe
LU1711	5/20/2016	Lung	67	Female	Right upper lobe nodule
LU1712	5/20/2016	Lung	69	Male	Ground-glass nodule, left upper lobe
LU1715	5/31/2016	Lung	70	Male	Lung carcinoma
LU1735	7/14/2016	Lung	70	Female	Right upper lobe lung cancer
LU1746	7/25/2016	Lung	69	Female	Adenocarcinoma, right lower lobe of lung
LU1749	8/1/2016	Lung	36	Male	Non-small cell lung cancer, left lung
LU1752	8/9/2016	Lung	73	Female	Mucinous cystic mass of the left lower lobe of the lung
LU1767	9/7/2016	Lung	55	Male	Probable lymphoma of lung
LU1807	10/11/2016	Lung	85	Male	Adenocarcinoma, left lower lobe of lung
LU1821	10/19/2016	Lung	64	Female	Metastatic sarcoma to left upper lobe of lung

LU1837	10/31/2016	Lung	56	Female	Right lower lobe lung carcinoma
LU1842	11/3/2016	Lung	60	Female	Left lower lobe lung cancer
LU1905	1/20/2017	Lung	72	Female	Left lung cancer
LU1926	2/3/2017	Lung	56	Female	Metastatic colon cancer to right upper lobe
LU1936	2/13/2017	Lung	79	Female	Lung carcinoma
LU1939	2/15/2017	Lung	44	Male	Metastatic renal cell cancer to left upper lobe of lung
TN1724	6/17/2016	Tonsil	3	Male	Adenotonsillar hypertrophy and sleep disordered breathing
TN1750	8/5/2016	Tonsil	5	Male	Sleep-disordered breathing; Adenotonsillar hypertrophy
TN1771	9/9/2016	Tonsil	3	Female	Sleep-disordered breathing; Adenotonsillar hypertrophy
TN1772	9/9/2016	Tonsil	4	Male	Adenotonsillar hypertrophy
TN1812	10/14/2016	Tonsil	3	Male	Sleep disorder breathing; Adenotonsillar hypertrophy
TN1813	10/14/2016	Tonsil	4	Female	Sleep-disordered breathing
TN1814	10/14/2016	Tonsil	6	Female	Recurrent strep pharyngitis
TN1869	12/2/2016	Tonsil	3	Female	Adenotonsillar hypertrophy and sleep disordered breathing
TN1870	12/2/2016	Tonsil	9	Male	Adenotonsillar hypertrophy
TN1882	12/2/2016	Tonsil	9	Male	Adenotonsillar hypertrophy
TN1887	12/2/2016	Tonsil	9	Male	Adenotonsillar hypertrophy
TN1888	12/2/2016	Tonsil	9	Male	Adenotonsillar hypertrophy

Table S2. Overview non-human primates used in this study. Related to Figure 5.

Animal	**TB Status**	**SIV Status**	Reference
FE10	LTBI	negative	Foreman et al 2016
FJ05	LTBI	negative	Foreman et al 2016
GP50	LTBI	negative	unpublished
HA90	LTBI	negative	Foreman et al 2016
HB74	LTBI	negative	Foreman et al 2016
HC90	LTBI	negative	Foreman et al 2016
HV02	LTBI	negative	unpublished
JD72	LTBI	negative	unpublished
JF47	LTBI	negative	unpublished
JK54	LTBI	negative	unpublished
JN75	LTBI	negative	unpublished
EH92	LTBI	positive	unpublished
HP22	LTBI	positive	Foreman et al 2016
HP41	LTBI	positive	Foreman et al 2016
ID91	LTBI	positive	Foreman et al 2016
IF04	LTBI	positive	unpublished
IP88	LTBI	positive	unpublished
JE48	LTBI	positive	unpublished
KG40	LTBI	positive	unpublished
ER44	ATB	positive	Foreman et al 2016
HB12	ATB	positive	Foreman et al 2016
HV08	ATB	positive	Foreman et al 2016
ID01	ATB	positive	Foreman et al 2016
JF23	ATB	positive	unpublished
JH07	ATB	positive	unpublished
JI68	ATB	positive	unpublished